Extensive Study of the Wobbling Properties in ^{163}Lu for the Positive and Negative Parity States

R. Poenaru *[1,2] and A. A. Raduta †[2,3]

[1]Doctoral School of Physics, University of Bucharest, Romania
[2]*Horia Hulubei* National Institute for Physics and Nuclear Engineering, Măgurele-Bucharest, Romania
[3]Academy of Romanian Scientists, Bucharest, Romania

April 8, 2021

Abstract

A new interpretation of the wobbling structure in ^{163}Lu is developed. Four wobbling bands are experimentally known in this isotope, where three are wobbling phonon excitations $TSD_{2,3,4}$, and the ground state band, which is TSD_1. In this work, a particle-triaxial rotor coupling is considered in a product space of single-particle and collective core states. The single-particle states describe a $j = i_{13/2}$ proton, while the core states characterize the triaxial rotor and are either of positive parity, when the bands $TSD_{1,2,3}$ are concerned or of negative parity for the TSD_4 band. There are five free parameters, three moments of inertia, the strength of the particle-core interaction, and the γ deformation. A very good description of all 62 experimental states is obtained, with a mean square error of about 80 keV. The system's stability dependence on energy is appraised in terms of a contour plot of the surface energy, while the dependence of classical trajectories on angular momentum as well as on energy is discussed by showing the intersections between the surfaces associated with the two constants of motion, i.e., the energy and the total angular momentum. This analysis suggests three different nuclear phases that emerge. The newly obtained features evidenced in the present work enrich the knowledge about the wobbling properties of ^{163}Lu.

1 Introduction

Triaxiality in nuclei has become an interesting topic for physicists over the years, mainly due to the large number of characteristics that become apparent from these kinds of shapes but also for its great challenge of measuring it experimentally. Moreover, stable triaxial shapes are of rare occurrence across the chart of nuclides [1], since the predominant character of nuclei is either spherical or axially symmetric. Over the last two decades, it has been shown that triaxiality plays a crucial role in measurements of important quantities like separation energies of the nucleons [1], and also fission barriers in heavy nuclei [2], however, concrete evidence of triaxiality in nuclei was still missing or under investigation. Tremendous work was given in finding a clear signature for non-axially symmetric shapes: effects such as anomalous signature splitting [3], signature inversion [4], and staggering of γ bands [5] were pointed out, but only recently two clear fingerprints of nuclear triaxiality have emerged in the literature, based on both experimental and theoretical findings. Indeed, the phenomena of *chiral symmetry breaking* [6] and that of *wobbling motion* (W.M.) [7] are considered as unique characteristics of nuclear triaxiality.

Chirality consists of the existence of a pair of chiral twin bands with an identical structure and almost similar energies. These bands are expected to appear due to the coupling of valence nucleons and the collective mode of rotation that could drive the total spin away from any of the three principal planes, giving rise to both left-handed and right-handed orientation of the angular momentum vectors [6]. A rigorous study of all the nuclei with chiral bands was done by Xiong and Wang [8], where reportedly a total of 59 chiral doublet bands in 47 such nuclei are confirmed. As a matter of fact, 8 of these nuclei have multiple chiral doublets. Several other studies were developed over the years, giving rise to new theoretical frameworks that accurately describe this phenomenon [9–14].

On the other hand, the experimental observations regarding wobbling motion have been quite rare, even though this kind of collective motion has been theoretically predicted almost 50 years ago by Bohr and Mottelson [7] when they were investigating the rotational modes of a triaxial nucleus employing a Triaxial Rotor Model

*E-mail: robert.poenaru@drd.unibuc.ro
†E-mail: raduta@nipne.ro

(TRM). Therein, it was shown that for a triaxial rotor, the main rotational motion is around the axis with the largest moment of inertia (MOI), as it is energetically the most favorable. This mode is quantum-mechanically disturbed by the rotation around the other two axes, since rotation around any of the three principal axes of the system are possible, due to the anisotropy between the MOIs (that is $\mathcal{I}_1 \neq \mathcal{I}_2 \neq \mathcal{I}_3$). Naturally, the description of the energy spectra and electromagnetic transitions between the rotational states of these wobbling nuclei (also known as *wobblers*) are considered to be the main characteristics that are put to the test by a theoretical investigation. The overall agreement between experimental results and the theoretically obtained data serves as an indicator for the quality of the model used to describe the wobbling picture. Regarding the experimental results for the known wobblers, this will be discussed in the next section, together with an overview of the recent progress made for the theoretical description of this type of nuclear motion.

The present work aims at extending the knowledge of the wobbling characteristics in an even-odd nucleus, which will be done by studying the energy spectrum of ^{163}Lu in a semi-classical approach, where the rotational states are described through a set of classical equations. In contradistinction with previous work, [15], in this formalism, all four wobbling bands are described by the same *core-quasiparticle alignment*, making thus the description of the wobbling motion consistent. A remarking feature for the current research is the introduction of the concept of *parity partner bands* - concerning the states from TSD_2 and TSD_4 bands - which will be discussed throughout the paper. Additionally, by studying the geometry of the triaxial rotor and that of the total angular momentum, some interesting characteristics of the wobbling motion will be pointed out.

This paper is organized as follows. In Section 2, a few theoretical aspects of WM will be mentioned, indicating some key points that the current study shall consider analyzing. Also in Section 2, experimental observations regarding WM in even-even and even-odd nuclei are presented, concluding the introductory part of the study. Following Section 3, a synopsis of the recent reinterpretation on the wobbling band structure for ^{163}Lu as described in [15] will be made. This will be the *core-idea* that serves as the foundation of the newly developed model introduced here. A direct comparison between this approach and the one from [15] is sketched, pointing out the improved features of the former. The theoretical formalism and the analytical formulas will be presented in Section 4. Experimental results concerning the wobbling spectrum of ^{163}Lu will be compared with the newly obtained data in Section 5. Finally, an outlook and conclusions are given in Section 6.

2 Wobbling motion in nuclei - experimental & theoretical overview

W.M. can be viewed as the quantum analogue for the motion of the asymmetric top, whose rotation around the axis with the largest MOI is energetically the most favored. A uniform rotation about this axis will have the lowest energy for a given angular momentum (spin). As the energy increases, this axis will start to precess with a harmonic type of oscillation about the space-fixed angular momentum vector, giving rise to a family of wobbling bands, each characterized by a wobbling phonon number n_w. The resulting quantal spectrum will be a sequence of rotational $\Delta I = 2$ bands, with an alternating signature number for each wobbling excitation. According to [7], it is possible to obtain the wobbling spectrum of any triaxial rigid rotor, by using the information related to its angular momentum I, moments of inertia $\mathcal{I}_{1,2,3}$, rotational frequency $\omega_{\rm rot}$, wobbling frequency $\omega_{\rm wob}$ as follows:

$$E_{\rm rot} = \sum_i \left(\frac{\hbar^2}{2\mathcal{I}_k}\right) I_k^2 \approx \frac{\hbar^2}{2\mathcal{I}_1} I(I+1) + \hbar\omega_{\rm wob}\left(n_w + \frac{1}{2}\right) \ , \tag{1}$$

with $\omega_{\rm wob}$ given by the following expression:

$$\hbar\omega_{\rm wob} = \hbar\omega_{\rm rot}\sqrt{\frac{(\mathcal{I}_1 - \mathcal{I}_2)(\mathcal{I}_1 - \mathcal{I}_3)}{\mathcal{I}_2\mathcal{I}_3}} \ , \tag{2}$$

where the rotational frequency of the rigid rotor is given by $\hbar\omega_{\rm rot} = \frac{\hbar I^2}{\mathcal{I}_1}$. In Eq. 1, the approximation of very large MOI along 1-axis is considered (i.e., $\mathcal{I}_1 >> \mathcal{I}_2, \mathcal{I}_3$), and $I(I+1) = I_1^2 + I_2^2 + I_3^2$. One can see that the wobbling motion is expressed as a 1-dimensional vibration with only one variable, since the energy of the zero-point fluctuation is $\frac{\hbar\omega_{\rm wob}}{2}$ [16].

Just for an illustrative purpose, Figure 1 shows a theoretical spectrum for the wobbling bands within a triaxial rigid rotor. The family of wobbling bands is obtained from a set of three moments of inertia (along the three principal axes), a given angular momentum, and increasing wobbling phonon numbers ($n_w = 0, 1, \dots$). Moreover, in Figure 1, the tilting of the angular momentum away from the rotational axis is sketched, where the tilt increases with the increase in the wobbling excitation. In a given sequence of wobbling bands, both the intra-band $\Delta I = 2$ as well as inter-band $\Delta I = 1$ transitions have a strong $E2$ collective character.

It is important to mention that the wobbling spectrum described by Eq. 1 and graphically represented in Figure 1 was firstly predicted for an even-even triaxial nucleus [7]. This predicted wobbling mode has not been

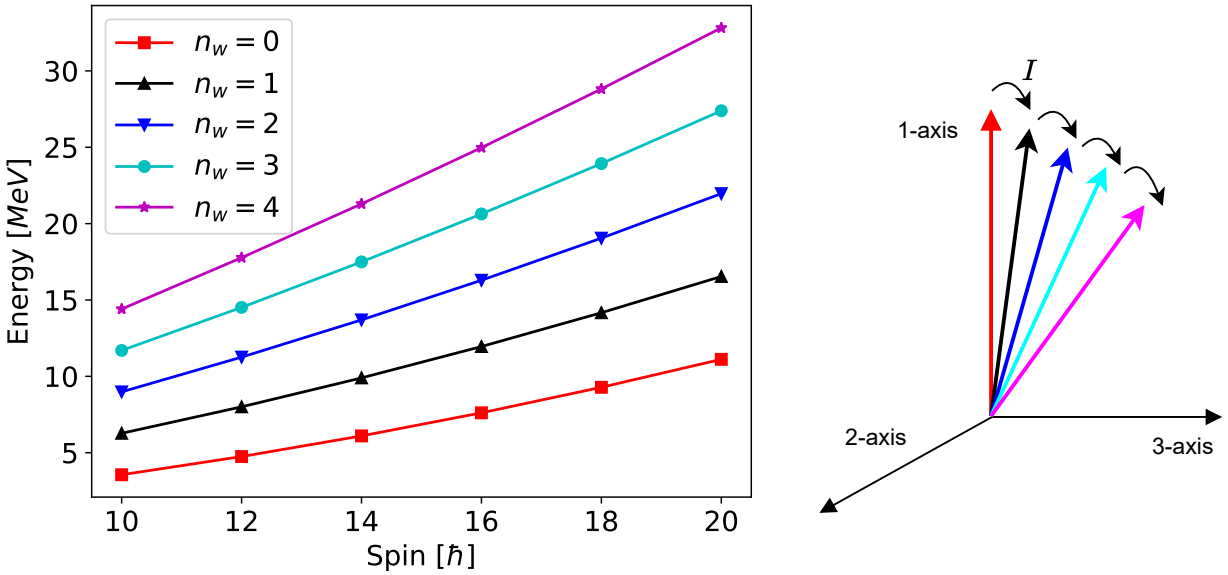

Figure 1: Family of wobbling bands for a simple triaxial rotor (left-side). Tilting of the angular momentum vector away from the rotational axis with an increase in spin (right-side). This schematic representation was done for an arbitrary set of MOIs $\mathcal{I}_1 : \mathcal{I}_2 : \mathcal{I}_3 = 25 : 5 : 2$.

experimentally confirmed yet. However, the first experimental evidence for wobbling excitations in nuclei was for an even-odd nucleus, namely ^{163}Lu, where a single one-phonon wobbling band was measured initially [17], followed by two additional wobbling bands discovered one year later [18, 19].

2.1 Experimental findings

After the first discovery of wobbling bands in ^{163}Lu ($Z = 71$), an entire series of even-odd isotopes with $A \approx 160$ were experimentally confirmed as *wobblers*: ^{161}Lu, ^{165}Lu, ^{167}Lu, and ^{167}Ta. In these nuclei, the wobbling mode appears due to the coupling of a valence nucleon (the so-called $\pi(i_{13/2})$ intruder) to a triaxial core, driving the entire nuclear system up to large deformation ($\epsilon \approx 0.4$) [20].

With time, several nuclei in which WM occurs were also found in regions of smaller A. Indeed, two isotopes with $A \approx 130$: ^{133}La [21] and ^{135}Pr [22, 23] were identified as having wobbling bands which emerge from the coupling of a triaxial even-even core with the $\pi(h_{11/2})$ nucleon for ^{135}Pr, and an additional pair of positive parity quasi-protons for ^{133}La. In the case of ^{133}La, the system is characterized as a longitudinal wobbler (it is in fact the first nucleus in which the longitudinal wobbling regime has been experimentally identified), while ^{135}Pr has a transverse wobbling regime. In both cases, the resulting coupling has a deformation $\epsilon = 0.16$ [21,22], which is smaller than the deformation in the heavier nuclei from the $A \approx 160$ region. A third nucleus that also lies in this mass region was confirmed very recently by Chakraborty et. al. in [24], namely the odd-A ^{127}Xe, where a total of four wobbling bands have been reported by the team (two yrast bands, and two excited phonon bands with $n_w = 1$ and $n_w = 2$). It is also suggested that ^{131}Ba could exhibit transverse wobbling [25] due to the alignment of a quasiparticle with hole-like character (the $h_{11/2}$ neutron), but in order to support this interpretation, the connecting transitions must show predominant $E2$ character.

Some additional progress was made in the $A \approx 100$ mass region, with experimental evidence for ^{105}Pd with two such bands that are built on a $\nu(h_{11/2})$ configuration, the first one so far in which a valence neutron couples to the triaxial core [26]. The resulting configuration drives the nuclear system up to deformation $\epsilon \approx 0.26$ and a transverse wobbling behavior.

The heaviest nuclei known so far in which WM has been experimentally observed are the isotopes $Z = 79$ with $A = 183$ [27] and $A = 187$ [28], respectively. However, for the case of ^{187}Au, there is an ongoing investigation [29] whether the two wobbling bands ($n_w = 0$ and $n_w = 1$) are bands with wobbling character, or if they are of magnetic nature (which would exclude the wobbling phonon interpretation). The nucleus ^{183}Au has probably the most interesting wobbling behavior, due to the appearance of both increasing and decreasing parts of the wobbling energy as a function of angular momentum, for states belonging to the same band (see Figure 5 from [27]). The experimental evidence for this nucleus shows that the positive parity band behave as a TW (despite the increasing behavior) due to the geometry of the coupling of the odd quasiparticle. This has important implications which will be discussed later on. For now, it is important to remember that there are cases where some transverse wobblers could be increasing functions of angular momentum, in the low-spin regions.

Regarding the wobbling motion for the even-even nuclei (behavior that was described in Figure 1), the experimental results are fragmentary, with scarce or unclear evidence on this collective behavior. However, some embryos of even-even wobblers have been reported in the recent years. For example, the ^{112}Ru ($Z = 44$) nucleus has three wobbling bands [30], two of them being the excited one- and two-wobbling phonon bands. Another nucleus is ^{114}Pd [31], with two excited bands of wobbling character, similar to ^{112}Ru. Indeed, for ^{112}Ru and ^{114}Pd the ground band together with the odd and even spin members of the γ-bands were interpreted as zero-(yrast), one-, and two-phonon wobbling bands. Unfortunately, since there are no data concerning the electromagnetic transitions, its wobbling character is still unclear. The even-even nucleus ^{130}Ba ($Z = 56$) [32–34] was confirmed very recently to exhibit wobbling behavior based on a two quasiparticle configuration with pair of bands with even and odd spins as zero- and one-phonon wobbling bands, respectively. What is worth noting for this case is the fact that these two bands are built on a configuration in which two aligned protons that emerge from the bottom of $h_{11/2}$ shell couple with the triaxial core. One remarks the change in nature of the wobbling motion from a purely collective form, but in the presence of two aligned quasiparticles [33], with a transverse wobbling character.

Concerning the interpretation of the energy spectrum for the wobbling motion which occurs in the nuclei that were mentioned above, it is mandatory to discuss some aspects related to its behavior with the increase in total angular momentum (nuclear spin). Thus, the concepts of *longitudinal wobblers* (LW) and *transverse wobblers* (TW) emerged from an extensive study done by Frauendorf et. al. [35] in which the team studied the possible coupling schemes that a valence nucleon can create with the triaxial core, giving rise to two possible scenarios. Based on microscopic calculations using the Quasi-Particle Triaxial Rotor (QTR) model, they showed that if the odd valence nucleon aligns its angular momentum vector $\vec{j}$ with the axis of largest MOI, the nuclear system is of longitudinal wobbling character. On the other hand, if the odd nucleon aligns its a.m. vector $\vec{j}$ with an axis perpendicular to the one with the largest MOI, then the nuclear system has a transverse wobbling character. Consequently, for LW the wobbling energy $E_{\rm wob}$ (see Eq. 3) has an *increasing* behavior with an increase in the angular momentum, while for TW the energy $E_{\rm wob}$ *decreases* with increasing angular momentum.

From the nuclei that were mentioned above, most of them are of TW type, with only ^{127}Xe [24], ^{133}La [21], and ^{187}Au [28] having an LW character. The energy that characterizes the type of wobbling in a nuclear system is the energy of the first excited band (the one-phonon $n_w = 1$ wobbling band) relative to the yrast ground band (zero-phonon $n_w = 0$ wobbling band):

$$E_{\rm wob}(I) = E_1(I) - \left(\frac{E_0(I+1) + E_0(I-1)}{2} \right) , \tag{3}$$

with 0 and 1 representing the wobbling phonon number n_w.

The odd nucleons that couple with the rigid triaxial core will influence the appearance of a particular wobbling regime (LW or TW). In all the wobblers, there is a proton from a certain orbital that is coupling with the core, except for the case of ^{105}Pd, where the valence nucleon is a neutron. The nature of the odd quasiparticle (i.e., particle or hole) and its "position" in the deformed j-shell (i.e., bottom or top) will determine whether its angular momentum $\vec{j}$ will align with the *short* (s) or *long* (l) axes of the triaxial rotor, respectively (with the notations short s, long l, and medium m for the axes of a triaxial ellipsoid). The reasoning behind this has to do with the minimization of the overall energy of the system: in the first case, a maximal overlap of its density distribution with the triaxial core will determine a minimal energy, while in the second case, a minimal overlap of the density distribution of the particle with the core will result in a minimal energy. Moreover, if the quasiparticle emerges from the middle of the j-shell, then it tends to align its angular momentum vector $\vec{j}$ with the *medium* (m) axis of the triaxial core. Figure 2 aims at depicting the type of alignment of a quasiparticle with the triaxial core.

As previously mentioned, for a given angular momentum, uniform rotation around the axis with the largest MOI corresponds to minimum energy. For a triaxial rotor emerging from a Liquid Drop, this is equivalent to rotation around the m axis. Therefore, Frauendorf [35] classified the LW as the situation when the odd nucleon will align its angular momentum along the m-axis, while TW being the situation where j is aligned perpendicular to the m-axis (with s- or l-axis alignment depending on the j-shell orbital from which the odd nucleon arises). It is worthwhile to mention the fact that the analysis done in Ref. [35] was performed within a so-called *Frozen Alignment* approximation, where the angular momentum of the odd particle $\vec{j}$ is rigidly aligned with one of the three principal axes of the triaxial ellipsoid (that is s-, l- or m-axis).

For a better understanding of the wobbling regimes in terms of angular momentum alignment, Figure 3 depicts three particular cases, namely a simple wobbler - inset A.0 (the case firstly developed by Bohr and Mottelson [7]), a longitudinal wobbler - inset A.1, and a transverse wobbler - inset A.2.

2.2 Theoretical interpretations of Wobbling Motion

In terms of its theoretical analysis, the wobbling motion has been studied using multiple models and interpretations. The Triaxial Particle Rotor Model (PRM) has been widely used over the recent years [7, 35–38], these

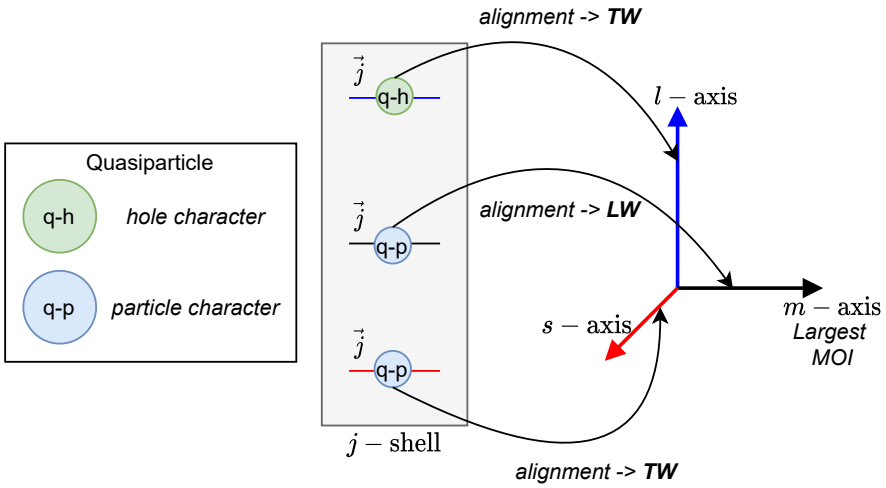

Figure 2: The wobbling regimes, Longitudinal Wobbling (LW) or Transverse Wobbling (TW), based on the type of alignment that an odd quasiparticle makes with the principal axes of a triaxial core. Each case depicts a coupling with an odd quasiparticle which emerges from the bottom/middle/top of a j-shell [35].

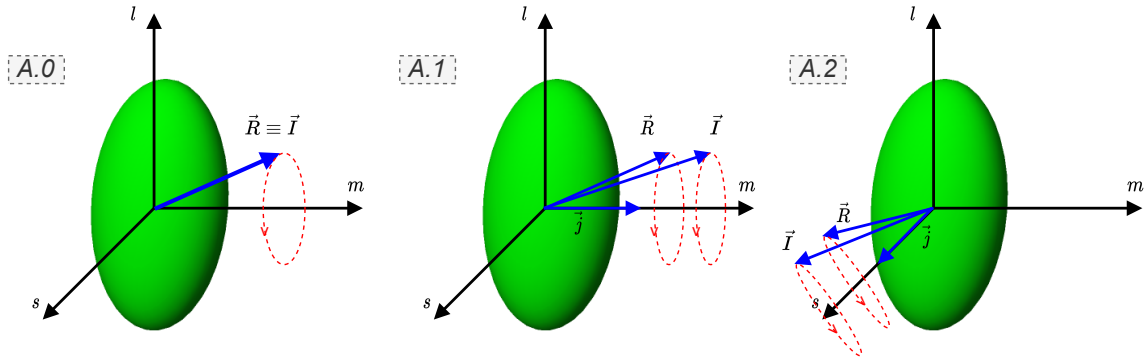

Figure 3: A.0: The geometry for the angular momentum of a simple wobbler. A.1: coupling geometry for a longitudinal wobbler (LW). A.2: coupling geometry for a transverse wobbler (TW). The short-s, long-l, and medium-m axes are defined in the body-fixed frame. The vectors $\vec{R}$, $\vec{j}$, and $\vec{I}$ represent the set of angular momenta of the core, odd particle, and the total nuclear system, respectively.

being quantal models that can be exactly solved in the laboratory frame. TRM was, however, firstly introduced for the motion of a rotating nuclear system by Davydov and Filippov in [39], where they obtained a complete quantal description for the motion of a triaxial nucleus (because the nucleus must have a well-defined potential minimum at a non-zero value for the triaxiality parameter γ). Starting from the framework of Cranking Mean Field Theory (CMFT), there were attempts at extending the cranking model for the study of WM. However, using the mean-field approximations, CMFT only helps at describing the yrast sequence for a given configuration. To improve that, the framework was extended with proper quantum correlations by incorporating the Random Phase Approximation (RPA) theory (see Refs. [40–47] for more details). The method of Collective Hamiltonian [48, 49] was used for the investigation of wobbling spectra in nuclei with the help of deformed potentials which were calculated from the Tilted Axis Cranking (TAC) model. TAC single j-shell model is also used for the description of the chiral vibrations and rotational motion in deformed nuclei [50, 51]. Mean-field approximations were also developed by the so-called *generator coordinate method after angular momentum projection* (GCM+AMP for short), with calculations that emerged from intrinsic cranking states [52]. Some analytical solutions were also developed (based on certain approximations), such as the harmonic approximation (HA) [7,35,48,53], Dyson boson expansion [53,54], and Holstein-Primakoff (HP) formula [37,53–56]. The angular momentum projections were also incorporated into the mean-field framework, with the recent development of a completely microscopic description of the wobbling motion by Shimada et. al. [57]. A Projected Shell Model (PSM) [58] which starts from the shell-model configuration mixing that is based on a Nilsson deformed mean field was also used for the theoretical study concerning WM. There are alternative developments based on the PSM approach, based on Density Functional Theories (DFT) that can be both non-relativistic [59] as well as relativistic [60].

Other tools that proved to be very efficient for the analysis of the wobbling nuclei are the semi-classical approaches, through which one can obtain equations of motion that describe the nuclear system quite well, starting from quantal Hamiltonians and further applying some de-quantization procedures. The semi-classical approach applied to generalized rotor Hamiltonians has the *advantage* of keeping close contact with the classical picture embedded in the dynamic of the systems. Recently, there has been quite an impressive progress towards realistic description of the wobbling motion [15, 35, 53, 61–64].

3 Re-interpretation of the wobbling bands in ^{163}Lu

Considered the *best wobbler* to date, ^{163}Lu has a rich wobbling spectrum [17, 18], with no less than four such wobbling bands: one yrast - TSD_1, (zero-phonon wobbling number $n_w = 0$), and three excited wobbling bands - $TSD_{2,3,4}$ (with their corresponding wobbling phonon numbers $n_w = 1, 2, 3$). The name TSD comes from Triaxial Strongly Deformed bands. The triaxial bands emerge due to the coupling of an odd-$\vec{j}$ nucleon with an even-even triaxial core. Thus, for ^{163}Lu, it is the intruder $\pi(i_{13/2})$ that couples to the triaxial core [17, 19, 36], driving the nuclear system up to large deformation, and stabilizing the deformed structure. Indeed, a triaxial shape with deformation parameters $(\epsilon_2, \gamma) \approx (0.38, +20^\circ)$ is assumed to be in agreement with the observed data, based on calculations using the Ultimate Cranker Code [65] for the potential energy surface (PES).

In terms of the experimental evidence which should be pointing out wobbling nature for the four TSD bands belonging to ^{163}Lu, the large transition quadrupole moment $Q_t \approx 10\ b$ [66], the predominantly $E2$ character of the transitions linking adjacent bands ($I \to I-1$), a large $E2/M1$ mixing ratio $\delta > 1$ for the transitions linking the yrare ($n_w = 1$) and yrast ($n_w = 0$) bands are all clear fingerprints of wobbling nature. For a set of results concerning these quantities (both theoretical and experimental), see Ref. [53], and the references cited therein. Another quantity that indicates strong deformation with wobbling character is the relative rigid rotor energy, and for this isotope, calculations show that all four bands have similar behavior with respect to this value (see Figures 3 and 4 from Ref. [67]).

Considering the experimental evidence which was indicated above and calculations based on particle rotor models, it can be summarized that the *generally accepted* formalism for the band structure in ^{163}Lu is the following:

- There are three excited wobbling bands (w.b.) TSD_2, TSD_3, and TSD_4 and one ground-state w.b. TSD_1.
- The three excited w.b. have wobbling-phonon numbers $n_{w_2} = 1$, $n_{w_3} = 2$, and $n_{w_4} = 3$, respectively.
- All three bands are built on top of the yrast state (the ground state band) with zero-wobbling-phonon number $n_{w_1} = 0$.
- Stable triaxial super-deformation is achieved due to the alignment of the odd $\pi(i_{13/2})$ nucleon which couples to a triaxially deformed core $\vec{R}$.

- $TSD_{1,2,3}$ have all positive parity $\pi_1 = \pi_2 = \pi_3 = +1$, while the spin states belonging to TSD_4 have negative parity $\pi_4 = -1$. All states within the four bands have a half-integer spin.

In accordance with the band structure which was just formulated, a fully semi-classical approach for the description of the wobbling spectrum of ^{163}Lu was by Raduta et. al. [53]. Therein, with the Time-Dependent Variational Equation (TDVE) applied on the PRM Hamiltonian and a trial wave-function that encapsulates both the states of the deformed nucleus I and the single-particle states j, a set of analytical expressions for the excitation energies of all four bands was obtained. The energies belonging to the excited wobbling phonons were populated by the action of a phonon operator $\Gamma^\dagger$ on the ground state. Indeed, by acting with the phonon operator on the ground state with the spin $I = R + j$ and $R = 0, 2, 4, \ldots$, the states from TSD_2 ($n_w = 1$) can be obtained. By applying twice ($n_w = 2$) the phonon operator, the rotational states from TSD_3 will be created. Lastly, the states from TSD_4 are obtained with the action on the ground state with three ($n_w = 3$) phonon operators: two of positive parity and one of negative parity (due to the overall negative parity $\pi_4 = -1$ of TSD_4). One has to remark the fact that for TSD_4, the model assumes an odd-particle-rotor-coupling with a different intruder: the $\pi(h_{9/2})$ nucleon. This was suggested by the negative parity orbital which might be occupied by this proton, in the spherical shell model. Several calculations in the literature point out that this nucleon might be causing the third excited wobbling band to have negative parity [68]. It is worthwhile mentioning that for the work described in [53], the variational principle was only applied for the states in TSD_1 since the other three wobbling bands are obtained through phononic excitations via the phonon operator $\Gamma^\dagger$.

In what follows, it is useful to introduce some notations that will refer to the formalisms developed in the present paper and the one formulated in [15] for the description of the wobbling motion in ^{163}Lu. As such, the study developed in [15] will be denoted with `W1`, while the current work will be shortly denoted by `W2`. For the sake of a self-consistent presentation, in subsection 3.1 a brief overview of the recently published work `W1` will be made, with further development of `W2` being presented in the subsection 3.2 - representing the *core concept* of the current analysis.

3.1 `W1` - Signature Partner Bands

Working with a semi-classical approach that is based on the triaxial particle rotor model, a full description of the wobbling bands for ^{163}Lu was achieved, but with a slightly modified band structure. Indeed, rather than applying a TDVE just for the yrast TSD_1 band, the states from TSD_2 were also obtained variationally. This was possible due to the different coupling schemes that emerged for TSD_1 and TSD_2, respectively. More precisely, in [15] and [64] there are three different coupling schemes ($\vec{R} + \vec{j}$): states from TSD_1 arise from the odd $\pi(i_{13/2})$ intruder coupling with a core with angular momentum sequence $R_1 = 0, 2, 4, \ldots$; states from TSD_2 arise from the same odd proton but coupling with a different triaxial core with angular momentum sequence $R_2 = 1, 3, 5, \ldots$. The band TSD_3 is obtained as a set of states which are built on top of TSD_2, with the action of an $n_w = 1$ wobbling quanta; this being different than the band structure previously mentioned were the third band was a two-phonon excitation of the yrast TSD_1. Lastly, the fourth band TSD_4 is a ground state band which results from the coupling of the same core as for TSD_2 (that is defined with the angular momentum sequence $R_2 = 1, 3, 5, \ldots$) but with a different odd nucleon: $\pi(h_{9/2})$. Consequently, TSD_2 and TSD_4 are yrast states, alongside TSD_1.

For the first three bands, the MOIs are the same, and they are considered to be free parameters within the numerical calculations. However, this is not true for the fourth band, where a different set of MOIs had to be introduced, since for TSD_4 the core polarization effects are changed by coupling scheme.

Using `W1`, the final results pointed out to the largest MOI corresponding to the 1-axis ($\mathcal{I}_1$ being the largest MOI obtained through the fitting procedure), making the system rotate around the 1-axis (that is the short s-axis). Moreover, the odd proton is aligned to the short axis as well, suggesting that the nucleus has an LW character. By representing the experimental wobbling energies according to Eq. 3, it was obtained that both the theoretical, as well as the experimental values were increasing functions of angular momentum (keep in mind that the first wobbling band $n_w = 1$ within the `W1` model is TSD_3). The agreement between the two sets of data (see Figure 6 from [64]) indicates that the condition for LW/TW character of the wobbling bands stated by Frauendorf et. al. in [35] is not strictly related to the increasing/decreasing wobbling energy E_{wob}. In fact, referring to the case of the wobbling motion for ^{183}Au, Nandi et. al. [27] also point out that the behavior of E_{wob} under spin increase should not be the only indicator of a certain wobbling regime, since for a larger spin interval (if there is experimental data available) there could be regions with both increasing and decreasing trends in wobbling energy. There is an ongoing debate whether the behavior of an LW or TW triaxial nucleus is strictly related to the change in E_{wob} with total a.m. [69–71].

A final aspect that needs to be mentioned regarding `W1` has to do with the interpretation of TSD_1 and TSD_2 as being Signature Partner Bands (SPB). Signature [7] is a quantum property that appears in deformed systems. It is strictly related to the invariance of a system with quadrupole deformation to a rotation by an

angle π around a principal axis. For example, a rotation around the x-axis will be defined as an operator:

$$\hat{R}_x = e^{i\pi \hat{I}_x} \ . \tag{4}$$

As for the framework used in [15, 64], due to the wave-function describing the system being written as a product between the $|I\rangle$ basis state corresponding to the total angular momentum and the single-particle basis state $|j\rangle$, the rotation operator used in `W1` achieves the following form:

$$\hat{R}_x(\pi) = e^{-i\pi \hat{I}_x} \otimes e^{-i\pi \hat{j}_x} \ . \tag{5}$$

If the system has axial symmetry, only the rotation around any of the principal axes that are perpendicular to the symmetry one can define the signature quantum number. Consequently, the signature is a property specific to a deformed system and it translates to a so-called *deformation invariance* with respect to space and time reflection properties [7]. For an even-even nucleus, the signature operator $\hat{R}_x$ has two eigenvalues, -1 and 1. For the even-odd case, the eigenvalues are $-i$ and $+i$, and depending on the total spin, the signatures can have two values, given by the following assignment:

$$\alpha_I = \frac{1}{2}\,(-1)^{I-1/2} \ . \tag{6}$$

Indeed, Eq. 6 describes the signature quantum number for a state of angular momentum I belonging to an odd mass nucleus. Such a rotational band with a sequence of states differing in spin by $\Delta I = 1$ will be divided into two branches, each branch consisting of levels differing in spin by $\Delta I = 2$, being related by the signature number $\alpha_I = \pm 1/2$. In [64] the signature concept is brought to the classical picture associated with a triaxial nucleus employing rotation operators which act on the trial function (this function is a product of two coherent states, one that is associated to the core and one to the valence nucleon). Eqs. 27-29 from [64] will extract two signatures for TSD_1 and TSD_2, namely the *favored* signature $\alpha_{1f} = +1/2$ for the first band, and *un-favored* signature $\alpha_{2u} = -1/2$ for the second band, respectively. A justification for the possibility of TSD_1 and TSD_2 of being SPB was based on the calculation of the triaxial potential (which was systematically performed in [53] and [62]), concluding that the minimum is very deep, preventing in this way the states from TSD_2 to share other minima through tunneling effects. Other experimental and theoretical results [72–75] for deformed nuclei around this mass region suggest that the calculations performed in `W1` regarding the connection between TSD_1 and TSD_2 as belonging to a signature splitting phenomenon are valid and consistent with already existing interpretations.

It is instructive to mention a few key-points which arise based on the above discussion regarding `W1`:

(a) The wobbling band structure in ^{163}Lu was re-interpreted: three bands are now yrast ground states, and only TSD_3 is one-phonon excited wobbling band (built on top of TSD_2)

(b) Both TSD_1 and TSD_2 are obtained variationally, by solving the time dependent variational equation associated to the initial quantal Hamiltonian

(c) There are three different $R + j$ coupling schemes that will produce the entire wobbling spectra of ^{163}Lu (the following naming scheme is exclusive to this work):

  (i) Coupling C_1: The odd proton $j_1 = 13/2$ is coupled to a core sequence with a.m. $R_1 = 0, 2, 4, \ldots$ (even spin states for the triaxial rotor).

  (ii) Coupling C_2: The same odd proton $j_1 = 13/2$ as in C_1 is coupled to a core sequence with a.m. $R_2 = 1, 3, 5, \ldots$ (odd spin states for the triaxial rotor).

  (iii) Coupling C_3: A different odd proton $j_2 = 9/2$ is coupled to the same core as in C_2.

(d) Two different sets of MOIs corresponding to the triaxial nucleus (that is the rotor coupled with the odd proton) are obtained as fitting parameters throughout the numerical calculations: one for the set $TSD_{1,2,3}$ and one for TSD_4.

(e) TSD_1 and TSD_2 are Signature Partner Bands: with TSD_1 (TSD_2) being the favored (un-favored) partner. Their corresponding signature quantum numbers are $\alpha_{1f} = +1/2$ and $\alpha_{2u} = -1/2$.

(f) As a side-by-side comparison with regards to the overall agreement with the experimental data, `W1` yielded better results when compared to the previous work depicted in Ref. [61], although it must be mentioned that both models are based on semi-classical approaches.

A diagram that shows the workflow involved in `W1` can be seen in Figure 15 from the Appendix. Also, a comparison with previous calculations can be seen in Figure 21 from Ref. [64].

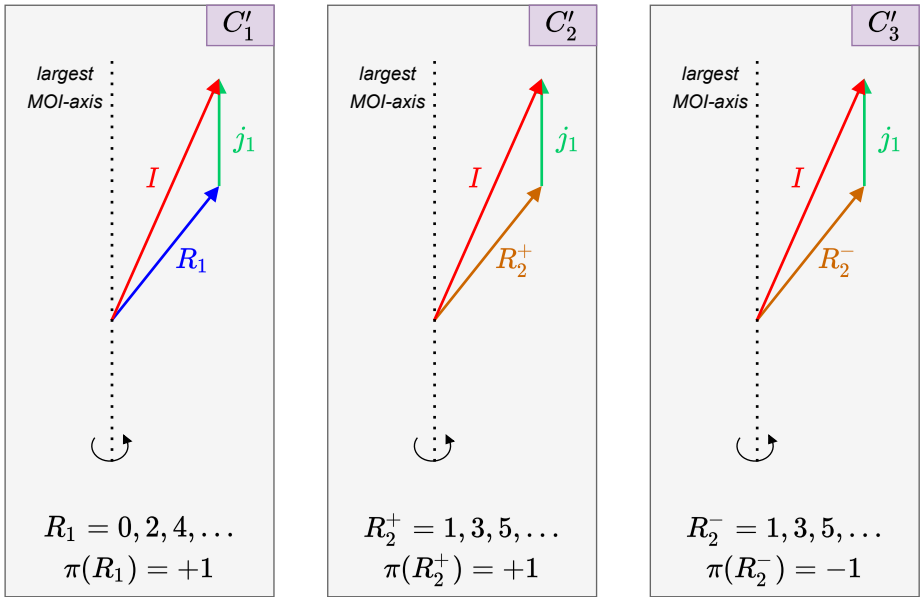

Figure 4: A schematic representation with the three coupling schemes that characterize the `W2` model. The same odd particle ($j_1 = i_{13/2}$ proton) is coupled with two positive cores with even (odd) integer spin sequences for TSD_1 (TSD_2), and one negative core in the case of TSD_4 with odd integer spin sequence. The total spin of the system precesses around the axis with the largest MOI, as it is the case for a triaxial rotor.

3.2 `W2` - Signature Partner Bands + Parity Partner Bands

The main question which can be asked regarding the formalism `W1` that was described in 3.1 is whether it is possible to obtain a *unified* description for all four bands in ^{163}Lu concerning the coupling scheme. In other words, it is worth investigating the possibility of having a unique single-particle state j that is coupled to a core of positive parity for the bands $TSD_{1,2,3}$ and a core of negative parity for TSD_4.

Fortunately, the answer is positive: starting from the semi-classical formalism of `W1`, one can properly adjust the coupling scheme, making sure that the entire numerical recipe used for obtaining the energy spectrum of ^{163}Lu remains consistent with the experimental results.

Regarding the unique single-particle that couples to the triaxial core, it is natural to pick the $i_{13/2}$ proton (that is j_1 from `W1`). The reasoning behind this choice has to do with the microscopic calculations [16, 19, 68] that showed stable triaxial structures in the ^{163}Lu potential energy surface when the triaxial core couples with a highly aligned j-shell particle, indicating the $\pi(i_{13/2})$ proton. Keep in mind that a highly aligned j-nucleon will *prefer* to keep a certain triaxial deformation when coupled to a core [76–78] (in the sense that the triaxiality parameter γ will have a certain value based on the orbital of the odd nucleon), and using microscopic calculations following the Ultimate Cranker code, it has been shown that a value of $\gamma \approx +20^\circ$ is preferred by the odd $\pi(i_{13/2})$ nucleon.

By taking $j = j_1$ as the sole intruder that couples to a positive core and also a negative core, the sequences with even/odd integer spins for the core do not change. In fact, the coupling schemes can be readily obtained:

(a) Coupling C'_1: the odd j_1 proton aligns with the core of even-integer spin sequence $R_1 = 0, 2, 4, \ldots$, with a parity of the R_1 core that is positive $\pi(R_1) = +1$.

(b) Coupling C'_2: the odd j_1 proton aligns with the core of even-integer spin sequence $R_2^+ = 1, 3, 5, \ldots$, with a parity of the R_2^+ core that is positive $\pi(R_2^+) = +1$.

(c) Coupling C'_3: the odd j_1 proton aligns with the core with an odd-integer spin sequence $R_2^- = 1, 3, 5, \ldots$, which has negative parity $\pi(R_2^-) = -1$.

From the three schemes defined above, it is clear that C'_1 corresponds to the yrast TSD_1, C'_2 to the ground state TSD_2, and finally C'_3 to the ground state TSD_4. Obviously, the odd valence nucleon j_1 has a positive parity $\pi_{j_1} = +1$. There has not been attributed a coupling scheme for TSD_3, since this band still remains as the one-wobbling phonon excitation that is built on top of TSD_2 with the action of a phonon operator which will be characterized later on. The three couplings are schematically represented in Figure 4. One should keep in mind the fact that $\vec{j}$ is aligned with the axis with the largest MOI does not necessarily mean the fact that the model works within the Frozen Alignment approximation - it is just an illustration.

The last step in searching for a unified coupling scheme in ^{163}Lu is to establish a possible relationship between the four bands. As per the calculations involved in `W1`, it was proven that signature is a good quantum number

and indeed, a sign that TSD_1 and TSD_2 are signature partners emerged. Their overall similar properties and spin difference enforce this argument. Furthermore, in this new `W2` approach, the difference in parity between the TSD_2 and TSD_4 but the same angular momentum sequence of their corresponding triaxial core R_2^+ and R_2^- strongly suggest that the two bands are *Parity Partner Bands*: two rotational sequences with energy states characterized by opposite parity, increasing energy that follows a trend $\propto I(I+1)$, and a spin difference $\Delta I = 2$ between states belonging to the same band. In the following section, calculations which will show that parity is indeed a good quantum number for the triaxial rotor + odd-particle system will be provided. For what it is worth mentioning now is that the concept of parity partners between TSD_2 and TSD_4 emerge from the idea that a stable strongly deformed structure is achieved from a single quasiparticle that moves in a quadrupole mean-field generated by a triaxial even-even core. However, there is a splitting in two different cases of coupling mechanisms, namely C_2'/C_3' depending on the alignment of the high-j-shell particle with a core of positive/negative parity.

Similar structures with alternating positive-negative parity bands have been also reported in other nuclei such as ^{40}Ca [79], or some heavier isotopes like ^{218}Fr [80]. In fact, a unified description of states with positive and negative parity in odd-mass nuclei was made over the last decade [81, 82], although therein, a quadrupole-octupole term was introduced within the particle-core Hamiltonian to describe this feature. A diagram which shows the workflow involved in `W2` can be seen in the Figure 16 from the Appendix A.

4 Theoretical Formalism

In this section, a description of the framework used for obtaining the wobbling spectrum of ^{163}Lu is made. As stated in the previous section, the system is described with a similar Hamiltonian used in `W1`, namely the Hamiltonian for the triaxial PRM.

$$H = H_{\text{core}} + H_{\text{s.p.}} \ . \tag{7}$$

The Hamiltonian from Eq. 7 describes a system in which an odd j particle interacts with a triaxial even-even core i.e., the odd nucleon is moving in a quadrupole deformed mean-field that is generated by the core. As such, the first term in the Hamiltonian H_{core} describes the motion of a triaxial core, while the second term $H_{\text{s.p.}}$ represents the single-particle potential characterizing the valence proton.

Indeed, the core Hamiltonian is given by:

$$H_{\text{core}} = \sum_{i=1,2,3} \frac{1}{2\mathcal{I}_i}(I_i - j_i)^2 \ , \tag{8}$$

where the core angular momentum is $\vec{R} = \vec{I} - \vec{j}$ and the terms $\mathcal{I}_i$ represent the moments of inertia for a triaxial ellipsoid, along the principal axes. These three moments of inertia will be considered as free parameters in the present calculations, but, compared to the work `W1`, a unique set of MOIs will be attributed to the four bands, since the triaxial core will create an alignment with a unique particle, that is j_1. Because of this, there is no option for their nature (i.e., rigid or hydrodynamic).

The single-particle Hamiltonian from Eq. 7 is derived from the well-known Nilsson potential [83, 84]:

$$h(\beta_2, \gamma) = C\left\{\cos\gamma Y_{20}(\theta,\varphi) + \frac{\sin\gamma}{\sqrt{2}}\left[Y_{22}(\theta,\varphi) + Y_{2-2}(\theta,\varphi)\right]\right\} \ , \tag{9}$$

where the coupling parameter C causes the level splitting in the deformed field and it is proportional to the quadrupole deformation β_2. The potential h from Eq. 9 is written in terms of the quadrupole deformation and triaxiality parameter that play the role of deformation parameters within a triaxial system (β_2, γ). Its expression using the coupling parameter C is widely used when working with a particle-rotor-model [85–87]. In the present this case, the change $h(\beta_2, \gamma) \rightarrow H_{\text{s.p.}}$ is done by applying the Wigner-Eckart theorem for the single-j particle, and the following expression for $H_{\text{s.p.}}$ will be obtained:

$$H_{\text{s.p.}} = \frac{V}{j(j+1)}\left[\cos\gamma(3j_3^2 - \vec{j}^2) - \sqrt{3}\sin\gamma(j_1^2 - j_2^2)\right] + \epsilon_j \ . \tag{10}$$

This term describes the motion of an odd particle with angular momentum j in a mean-field generated by a triaxial core, with a potential strength V characterized by the quadrupole deformation ($V \propto \beta_2$). In fact, the single-particle potential strength V will be considered as the fourth free parameter within the calculations and its behavior will dictate the coupling of the j particle with all four TSD bands. The term ϵ_j from Eq. 10 represents the single-particle energy that corresponds to the odd j proton from the i-orbital. One should not mix up the j_1 proton notation used throughout the paper with the components of the single-particle angular momentum from Eq. 10.

Regarding the triaxial deformation γ which enters in Eq. 10, its value will be considered as another free parameter of the current problem. In other words, having V and γ as free parameters means that the system will be described by its deformation parameters which will be obtained through a fitting procedure, keeping an agreement with the experimental data regarding the excitation energies of the rotational states belonging to $TSD_{1,2,3,4}$.

From Eqs. 8 and 10, the free parameter set can be obtained, hereafter denoted by $\mathcal{P}$. It comprises three moments of inertia, the single-particle potential strength, and the triaxial deformation. As such, $\mathcal{P}$ can be written as:

$$\mathcal{P} = [\mathcal{I}_1, \mathcal{I}_2, \mathcal{I}_3, V, \gamma] \ . \tag{11}$$

Solving the problem of `W2` is equivalent to finding the eigenvalues of H given in Eq. 7. In a similar approach as in `W1`, the eigenvalues of interest are obtained on the base of a semi-classical approach. Thus, the first step is to perform a de-quantization procedure on H through a TDVE [53, 61, 63]:

$$\delta \int_0^t \langle \Psi_{IjM} | \, H - i \frac{\partial}{\partial t'} \, | \Psi_{IjM} \rangle \, dt' = 0 \ . \tag{12}$$

Working within a semi-classical approach allows one to keep close contact with the system's dynamics in terms of equations of motion for the generalized coordinates. The trial function from Eq. 12 is carefully chosen as a product of two basis states comprising the states with total angular momentum I and j, respectively:

$$|\Psi_{IjM}\rangle = \mathbf{N} e^{z\hat{I}_-} e^{s\hat{j}_-} \, |IMI\rangle \, |jj\rangle \ , \tag{13}$$

where the operators $\hat{I}_-$ and $\hat{j}_-$ denote the lowering operators for the intrinsic angular momenta $\vec{I}$ and $\vec{j}$, respectively, and $\mathbf{N}$ plays the role of the normalization constant. One must remark the fact that the states $|IMI\rangle$ and $|jj\rangle$ from Eq. 13 are extremal states for the operators $(\hat{I}^2, \hat{I}_3)$ and $(\hat{j^2}, \hat{j}_3)$, respectively, and they correspond to the maximally allowed states for a given set of angular momenta I and j. As an observation, the trial function is an admixture of components of definite K, which is consistent with the fact that for a triaxial nucleus, K is not a good quantum number.

The variables z and s from Eq. 13 are complex functions of time, and they play the role of classical coordinates in the phase spaces that describe the motion of the core and the odd particle:

$$z = \rho e^{i\varphi} \ , \ s = f e^{i\psi} \ . \tag{14}$$

In order to obtain a set of classical equations in a Hamilton Canonical form, a new pair of variables are introduced:

$$r = \frac{2I}{1+\rho^2} \ , \ t = \frac{2j}{1+f^2} \ , \tag{15}$$

where $r \in [0, 2I]$ and $t \in [0, 2j]$.Thus the equations of motion acquire the form:

$$\begin{aligned} \frac{\partial \mathcal{H}}{\partial r} &= \dot{\varphi} \ ; \ \frac{\partial \mathcal{H}}{\partial \varphi} = -\dot{r} \ , \\ \frac{\partial \mathcal{H}}{\partial t} &= \dot{\psi} \ ; \ \frac{\partial \mathcal{H}}{\partial \psi} = -\dot{t} \ . \end{aligned} \tag{16}$$

The function $\mathcal{H}$ denotes the average of the Hamiltonian operator H (Eq. 7) with the trial function $|\Psi_{IjM}\rangle$ given in Eq. 13, and it plays the role of classical energy:

$$\mathcal{H}(\varphi, r; \psi, t) = \langle \Psi_{IjM} | \, H \, | \Psi_{IjM} \rangle \ , \tag{17}$$

Starting from the equations of motion given in Eq. 16, one can observe that the function $\mathcal{H}$ is a constant of motion, that is $\dot{\mathcal{H}} \equiv 0$. This equation will define a surface, a so-called equi-energy surface $\mathcal{H} = \text{const}$. It is worth mentioning the fact that such equality holds since the entire set of equations of motion emerged from a variational principle. The sign of the Hessian associated to this classical function will indicate its stationary points. Among them, some are minima. The critical points which are of interest for the present study are those obtained when the following ordering for the three moments of inertia holds: $\mathcal{I}_1 > \mathcal{I}_2 > \mathcal{I}_3$. There is no restriction on γ.

With a linearization procedure for the equations of motion around the minimum point of $\mathcal{H}$, a dispersion equation will be obtained:

$$\Omega^4 + B\Omega^2 + C = 0 \ . \tag{18}$$

The above equation describes a harmonic type of motion for the nuclear system, with the solutions to this algebraic equation as the *wobbling frequencies* Ω. The terms B and C are functions of total angular momentum I, single-particle a.m. j, inertial parameters $A_k = 1/(2\mathcal{I}_k)$, $k = 1, 2, 3$, single-particle potential strength V, and triaxiality parameter γ. The B term from Eq. 18 has the expression [64]:

$$-B = [(2I-1)(A_3 - A_1) + 2jA_1]\,[(2I-1)(A_2 - A_1) + 2jA_1] + 8A_2A_3Ij + \mathrm{T}^1_B\mathrm{T}^2_B \ , \tag{19}$$

where the terms T^1_B and T^2_B are defined defined as:

$$\begin{aligned}
\mathrm{T}^1_B &= \left[(2j-1)(A_3 - A_1) + 2IA_1 + V\frac{2j-1}{j(j+1)}\sqrt{3}(\sqrt{3}\cos\gamma + \sin\gamma)\right] \ , \\
\mathrm{T}^2_B &= \left[(2j-1)(A_2 - A_1) + 2IA_1 + V\frac{2j-1}{j(j+1)}2\sqrt{3}\sin\gamma\right] \ .
\end{aligned} \tag{20}$$

Accordingly, the C term from Eq. 18 has the expression [64]:

$$\begin{aligned}
C = &\left\{[(2I-1)(A_3 - A_1) + 2jA_1]\,\mathrm{T}^1_C - 4IjA_3^2\right\} \\
&\times \left\{[(2I-1)(A_2 - A_1) + 2jA_1]\,\mathrm{T}^2_C - 4IjA_2^2\right\} \ ,
\end{aligned} \tag{21}$$

where the terms T^1_C and T^2_C are defined defined as:

$$\begin{aligned}
\mathrm{T}^1_C &= \left[(2j-1)(A_3 - A_1) + 2IA_1 + V\frac{2j-1}{j(j+1)}\sqrt{3}(\sqrt{3}\cos\gamma + \sin\gamma)\right] \ , \\
\mathrm{T}^2_C &= \left[(2j-1)(A_2 - A_1) + 2IA_1 + V\frac{2j-1}{j(j+1)}2\sqrt{3}\sin\gamma\right] \ .
\end{aligned} \tag{22}$$

It can be seen that the terms which enter in B and C, namely $(\mathrm{T}^1_B, \mathrm{T}^2_B)$ from Eq. 20 and $(\mathrm{T}^1_C, \mathrm{T}^2_C)$ from Eq. 22 correspond to the quadrupole deformation that causes the single-particle to move in the mean-field of the triaxial core. The terms also define the triaxiality that the nucleus achieves once the odd proton couples to the triaxial core, driving the system up to a large (and stable) deformation.

Going back to Eq. 18, under the restrictions for the MOIs defined above, the dispersion equation admits two real and positive solutions (hereafter denoted with Ω^I_1 and Ω^I_2, where $\Omega^I_1 < \Omega^I_2$) defined for $j_1 = i_{13/2}$, given by:

$$\Omega^I_{1,2} = \sqrt{\frac{1}{2}\left(-B \mp (B^2 - 4C)^{1/2}\right)} \ . \tag{23}$$

These two solutions are interpreted as *wobbling frequencies* associated with the motion of the core, and the motion of the odd-particle respectively. As such, each wobbling frequency has an associated wobbling-phonon number:

$$\Omega^I_1 \to n_{w_1} \ ; \ \Omega^I_2 \to n_{w_2} \ . \tag{24}$$

Now the analytical expressions for the four TSD bands in ^{163}Lu are readily obtained:

$$\begin{aligned}
E^I_{\mathrm{TSD1}} &= \epsilon_j + \mathcal{H}^{(I,j)}_{\mathrm{min}} + \mathcal{F}^I_{00} \ , \ I = 13/2, 17/2, 21/2 \ldots \\
E^I_{\mathrm{TSD2}} &= \epsilon^1_j + \mathcal{H}^{(I,j)}_{\mathrm{min}} + \mathcal{F}^I_{00} \ , \ I = 27/2, 31/2, 35/2 \ldots \\
E^I_{\mathrm{TSD3}} &= \epsilon_j + \mathcal{H}^{(I-1,j)}_{\mathrm{min}} + \mathcal{F}^{I-1}_{10} \ , \ I = 33/2, 37/2, 41/2 \ldots \\
E^I_{\mathrm{TSD4}} &= \epsilon^2_j + \mathcal{H}^{(I,j)}_{\mathrm{min}} + \mathcal{F}^I_{00} \ , \ I = 47/2, 51/2, 55/2 \ldots \ ,
\end{aligned} \tag{25}$$

where $\mathcal{F}^I_{n_{w_1}n_{w_2}}$ is a function of the wobbling frequencies:

$$\mathcal{F}^I_{n_{w_1}n_{w_2}} = \Omega^I_1\left(n_{w_1} + \frac{1}{2}\right) + \Omega^I_2\left(n_{w_2} + \frac{1}{2}\right) \ , \tag{26}$$

and $\mathcal{H}^{(I,j)}_{\mathrm{min}}$ is the classical energy evaluated in its minimal point. For the present case, its analytical expression is given by the following equation:

$$\mathcal{H}^{(I,j)}_{\mathrm{min}} = (A_2 + A_3)\frac{I+j}{2} + A_1(I-j)^2 - V\frac{2j-1}{j+1}\sin\left(\gamma + \frac{\pi}{6}\right) \ . \tag{27}$$

Band	n_{w_1}	n_{w_2}	π	α	Coupling scheme
TSD_1	0	0	+1	+1/2	C'_1
TSD_2	0	0	+1	-1/2	C'_2
TSD_3	1	0	+1	+1/2	Built on top of TSD_2
TSD_4	0	0	-1	-1/2	C'_3

Table 1: The wobbling phonon numbers, parities, signatures, and coupling schemes assigned to each triaxial band in ^{163}Lu, within the `W2` model. The three coupling schemes were defined in Section 3.2.

A few aspects regarding the energy spectrum defined in Eq. 25 are worth mentioning. To each band, there is a specific energy ϵ_j associated with the single-particle state. In this case, the odd-proton $j_1 = 13/2$ from the i-orbital is the one that couples to the triaxial core. However, for the bands TSD_2 and TSD_4, a different re-normalization of ϵ_j is considered, since TSD_2 is the unfavored signature partner of TSD_1, and TSD_4 is the negative parity partner of TSD_2 within the band structure. These quantities will shift the overall energy states belonging to the two bands, each by a different amount. As a result, both ϵ_j^1 and ϵ_j^2 will be adjusted throughout the numerical calculations such that the energy spectrum is best reproduced. Another aspect concerns the band TSD_3; since this is the only excited wobbling band within the family, its configuration is built on top of TSD_2, with the action of a single phonon ($n_{w_1} = 1$) operator. Consequently, an energy state I belonging to TSD_3 is obtained from a state $I - 1$ from TSD_2. In Table 1, the rest of the wobbling phonon numbers are mentioned, with the parity, signature, and coupling scheme for each band in particular.

4.1 Parity quantum number for the wave-function

In `W1` it was shown that signature emerges from the calculations on the total wave-function as a good quantum number for this triaxial system. This is why in [64] the bands TSD_1 and TSD_2 appeared as Signature Partner Bands (SPB). In `W2`, such property still stands.

Since the backbone of the current work started from the need for a single odd-particle that couples to a triaxial core in ^{163}Lu, one has to look at the band TSD_4 (which was interpreted as having a different nucleon: j_2 with $j = 9/2$ from the h-orbital), and see if its differentiating properties can be linked to *main group* of bands (namely $TSD_{1,2,3}$). Indeed, from the experimental measurements regarding spin and parity assignment [68], it turns out that the parity of the rotational states is negative. Therefore, a forensic analysis on this quantum property should be considered as the necessary ingredient in a unified description of all four bands.

The parity operator is defined as a product of the complex conjugation operation and a rotation of angle π around the 2-axis: $P = e^{-i\pi\hat{I}_2}C$. The total parity operator is the product of an operator corresponding to the core and one corresponding to the single-particle:

$$\mathcal{P}_T = P_{\text{core}} P_{\text{s.p.}} \ . \tag{28}$$

Acting with the total parity operator defined above, on the trial function Ψ associated , the following result is obtained:

$$\mathcal{P}_T \Psi(r, \varphi; t, \psi) = \Psi(r, \varphi + \pi; t, \psi + \pi) \overset{\text{not.}}{=} \bar{\Psi}. \tag{29}$$

The classical energy function $\mathcal{H}$ has an invariance property at changing the angles with π:

$$\mathcal{H}(r, \varphi; t, \psi) = \mathcal{H}(r, \varphi + \pi; t, \psi + \pi) \ . \tag{30}$$

From Eqs. 29 and 30, it can be concluded that the wave-function describing the triaxial system Ψ and its image through $\mathcal{P}_T$, $\bar{\Psi}$, are two linearly dependent functions which differ only by a multiplicative constant p, with $|p| = 1$. Thus, p can either be -1 or +1, such that:

$$\bar{\Psi} = \pm\Psi(r, \varphi; t, \psi) \ . \tag{31}$$

The above result concludes the parity analysis for the wave-function, showing that the triaxial rotor admits eigenfunctions of negative parity. Therefore, a single wave-function characterized by the coupling of a triaxial core to the odd proton $i_{13/2}$ is describing both positive parity states ($\in TSD_{1,2,3}$) as well as negative parity states ($\in TSD_4$). This analysis, together with the fact that TSD_2 and TSD_4 have the same a.m. sequences (although TSD_2 has more states with low spin than TSD_4) suggest the fact that these two bands might be Parity Partners.

4.2 Energy function - geometrical interpretation

The analytical expression for the average of H with the trial function describing the system was previously calculated in `W1`. Indeed, the energy function $\mathcal{H}$ was given in terms of the phase space coordinates $(r, \varphi; t, \psi)$ as follows [64]:

$$\begin{aligned}\mathcal{H} =& \frac{I}{2}(A_1 + A_2) + A_3 I^2 + \frac{2I-1}{2I} r(2I-r)\mathcal{A}_\varphi + \frac{j}{2}(A_1 + A_2) + A_3 j^2 + \frac{2j-1}{2j} t(2j-t)\mathcal{A}_\psi \\ & - 2\sqrt{r(2I-r)t(2j-t)}\mathcal{A}_{\varphi\psi} + A_3\left[r(2j-t) + t(2I-r)\right] - 2A_3 Ij + V\frac{2j-1}{j+1}\mathcal{A}_\gamma \ , \end{aligned} \tag{32}$$

with:

$$\begin{aligned}&\mathcal{A}_\varphi(\varphi) = (A_1\cos^2\varphi + A_2\sin^2\varphi - A_3) \ , \\ &\mathcal{A}_{\varphi\psi}(\varphi,\psi) = (A_1\cos\varphi\cos\psi + A_2\sin\varphi\sin\psi) \ , \\ &\mathcal{A}_\psi(\psi) = (A_1\cos^2\psi + A_2\sin^2\psi - A_3) \ , \\ &\mathcal{A}_\gamma(t,\psi) = \left[\cos\gamma - \frac{t(2j-t)}{2j^2}\sqrt{3}(\sqrt{3}\cos\gamma + \sin\gamma\cos 2\psi)\right] \ . \end{aligned} \tag{33}$$

It is instructive to check the dependence of the energy function on the angular momentum components, e.g., the coordinates $x_k \overset{\text{not.}}{=} I_k \ , \ k = 1,2,3$, where the quantization axis is chosen as the 3-axis. By expressing the angular momentum coordinates $x_{1,2,3}$ in terms of the polar angles (θ, φ) and a radius I , one obtains:

$$x_1 = I\sin\theta\cos\varphi \ , \ x_2 = I\sin\theta\sin\varphi \ , \ x_3 = I\cos\theta \ . \tag{34}$$

Within this spherical coordinates, and evaluating the energy function around its minimum point $p_0 = (0, I; 0, j)$, the following expression for $\mathcal{H}$ results:

$$\mathcal{H}\mid_{p_0} = I\left(I - \frac{1}{2}\right)\sin^2\theta(A_1\cos^2\varphi + A_2\sin^2\varphi - A_3) - 2A_1 Ij\sin\theta + T_{\text{core}} + T_{\text{s.p.}} \ . \tag{35}$$

The last two terms in this equation are independent on the polar angles (θ, φ), and have the form:

$$\begin{aligned}T_{\text{core}} &= \frac{I}{2}(A_1 + A_2) + A_3 I^2 \ , \\ T_{\text{s.p.}} &= \frac{j}{2}(A_2 + A_3) + A_1 j^2 - V\frac{2j-1}{j+1}\sin\left(\gamma + \frac{\pi}{6}\right) \ . \end{aligned} \tag{36}$$

The classical equations of motion admit two constants of motion: the total energy (E) and the total angular momentum (I). Consequently, by finding the intersection line(s) between the surface of the energy ellipsoid E and the surface of the angular momentum, a sphere of radius I, one finds the system trajectory. Such representations will be made in the following section.

The expression of the energy ellipsoid in Cartesian coordinates is:

$$\begin{aligned}E =& \left(1 - \frac{1}{2I}\right)A_1 x_1^2 + \left(1 - \frac{1}{2I}\right)A_2 x_2^2 + \left[\left(1 - \frac{1}{2I}\right)A_3 + A_1\frac{j}{I}\right]x_3^2 - \\ & - I\left(I - \frac{1}{2}\right)A_3 - 2A_1 Ij + T_{\text{rot}} + T_{\text{sp}} \ . \end{aligned} \tag{37}$$

For a total angular momentum $\vec{I}$, the vector generates a sphere of radius $r = I$ described by the equation:

$$I^2 = x_1^2 + x_2^2 + x_3^2 \ . \tag{38}$$

The trajectories obtained through the intersection of Eqs. 37 and 38 will show a classical visualization of the wobbling character for a triaxial nucleus.

5 Numerical results

As a first step, the results concerning the excited spectrum of the four TSD bands will be presented. Regarding the wobbling spectrum of ^{163}Lu, its analytical formulation was given in Eq. 25. As mentioned, those energies

Band	n_s	$\vec{j}$	$\vec{R}$ - Sequence	$\vec{I}$ - Sequence	Coupling scheme
TSD_1	21	j_1	$R_1 = 0, 2, 4, \ldots$	$13/2, 17/2, 21/2, \ldots$	C_1'
TSD_2	17	j_1	$R_2^+ = 1^+, 3^+, 5^+, \ldots$	$27/2, 31/2, 35/2, \ldots$	C_2'
TSD_3	14	j_1	1-phonon excitation	$33/2, 37/2, 41/2, \ldots$	1-phonon excitation
TSD_4	11	j_1	$R_2^- = 1^-, 3^-, 5^-, \ldots$	$47/2, 51/2, 55/2, \ldots$	C_3'

Table 2: The number of energy states n_s within each wobbling band, the a.m. of the proton $\vec{j}$, the core's a.m. $\vec{R}$, the nucleus' a.m. $\vec{I}$, and the corresponding coupling scheme that was established according to the `W2` model. The single-particle is the $j_1 = (i_{13/2})$ proton.

$\mathcal{I}_1$ [$\hbar^2$/MeV]	$\mathcal{I}_2$ [$\hbar^2$/MeV]	$\mathcal{I}_3$ [$\hbar^2$/MeV]	γ [deg.]	V [MeV]
72	15	7	22	2.1

Table 3: The parameter set $\mathcal{P}$ that was determined by a fitting procedure of the excitation energies for ^{163}Lu.

are parametrized in terms of $\mathcal{P}$, which is the set of free parameters to be determined. Indeed, one can find $\mathcal{P}$ by minimizing the χ^2 function:

$$\chi^2 = \frac{1}{N_T} \sum_i \frac{(E_{\rm exp}^{(i)} - E_{\rm th}^{(i)})^2}{E_{\rm exp}^{(i)}} \ , \tag{39}$$

where N_T represents the total number of states. Table 2 contains the number of states within each band, with the spin sequences for the core ($\vec{R}$), the spin sequences for the coupled system (that is the total angular momentum $\vec{I}$), and the coupling schemes specific to `W2` formalism that is used in the current calculations.

The resulting values for $\mathcal{P}$ are given in Table 3. This `W2` method contrasts the approach in `W1`, where a second minimization process was needed separately for TSD_4. The root mean square error provided by the obtained parameter set $\mathcal{P}$ has a value of $E_{\rm rms} \approx 79$ keV. This result is much better than the one obtained with previous formalism `W1` where an $E_{\rm rms} \approx 240$ keV was obtained [64]). As a matter of fact, this is the first semi-classical formalism in the literature that achieves agreement with the experimental data with less than 100 keV for the entire wobbling spectrum of ^{163}Lu. It is worth mentioning that the fitting procedure was done not for the absolute wobbling energies $E^I_{\rm TSDk}$, $k = 1, 2, 3, 4$, but for the *excitation energies* which are relative to the hand-head $I = 13/2^+$ from the first yrast band TSD_1. Comparison between the theoretical values obtained within the current formalism and the experimental data is shown in Figures 5 and 6. For the sake of completeness, the wobbling frequencies which enter in the expression of the $\mathcal{F}^I_{n_{w_1} n_{w_2}}$ given by Eq. 26 are graphically represented as functions of total angular momentum I in Figure 7, for the fixed parameter set. It is remarkable the fact that the wobbling frequency Ω_2^I is much larger than its partner, suggesting the fact the coupling effects caused by the highly aligned proton have a stronger influence in achieving a wobbling character for ^{163}Lu, which is in line with the characteristics of a particle-rotor coupling. Another feature of these wobbling frequencies is their linear behavior with respect to the nuclear spin.

Concerning the single-particle energies from Eq. 25, namely ϵ_j^1 and ϵ_j^2 that emerge from the un-favored signature of TSD_2 and negative parity of TSD_4, respectively, they induce a correction for the mean-field with the quantities $\epsilon_j^1 - \epsilon_j = 0.3$ MeV and $\epsilon_j^2 - \epsilon_j = 0.6$ MeV. Note that since the energy state $I_{13/2} \in TSD_1$ (the band-head of TSD_1) was subtracted from all bands, the single-particle energies for band 2 and 4 are adjusted accordingly.

The quantity $\epsilon_j^1 - e_j$ is added to the second band due to the core, and such a splitting is caused by the fact that two distinct TDVE procedures were performed for the two partner bands $TSD_{1,2}$. The total signature splitting for the band-head and the terminus states of TSD_2 are $E^{27/2}_{TSD2} - E^{25/2}_{TSD2} = 0.492$ MeV and $E^{91/2}_{TSD2} - E^{89/2}_{TSD2} = 0.936$ MeV which agrees with the estimate made by Jensen et. al. in [19]. Although the signature splitting can be determined microscopically by using a deformed single-particle basis amended with a cranking constraint, for the present case it is obtained by applying the TDVE for each spin state and the correction corresponding to the single-particle energies (that is ϵ_j^1).

Another noteworthy aspect of the current formalism is the fact that the difference $\delta_{42} = E^I_{\rm TSD4} - E^I_{\rm TSD2}$ for all the states has an almost constant value $\delta_{42} \approx 0.3$ MeV. This suggests that the states of the same a.m. from TSD_2 and TSD_4 bands might emerge through the parity projection of a sole wave-function that does not have reflection symmetry. In the present case, this is caused by the fact that the wobbling frequency is parity-independent. It is interesting that the action of the parity operator on any rotational state within the angular momentum space will lead to the change of the angular momentum vector from $\vec{I}$ to $-\vec{I}$. Due to this reason, the parity operator commutes with the initial Hamiltonian, and the eigenfunctions of H are characterized by either positive or negative parity (with states of different parities being degenerate). However, one can lift this

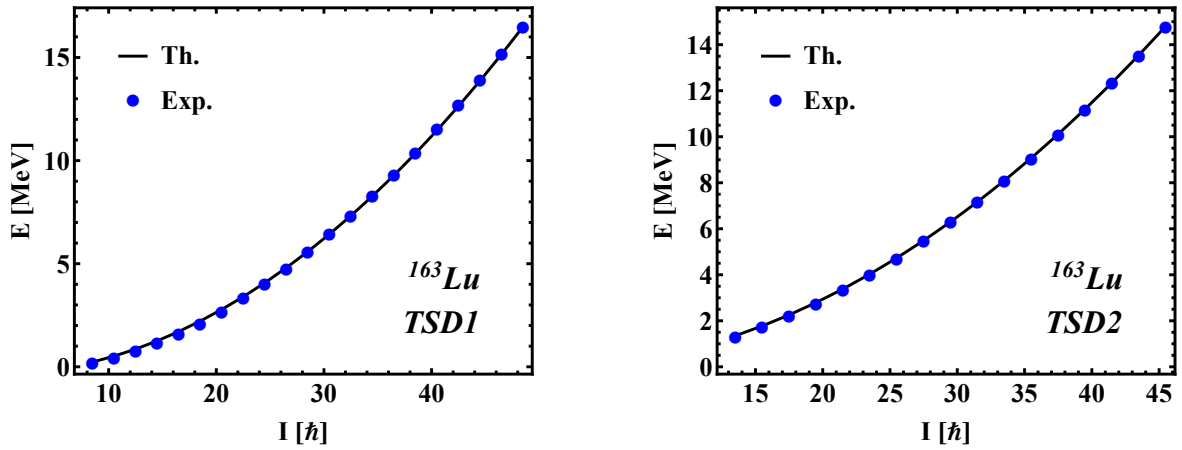

Figure 5: Comparison between theoretical and experimental excitation energies for the first two wobbling bands in ^{163}Lu within the W2 model. The theoretical results are obtained with the parameters listed in Table 3. Experimental data is taken from [88].

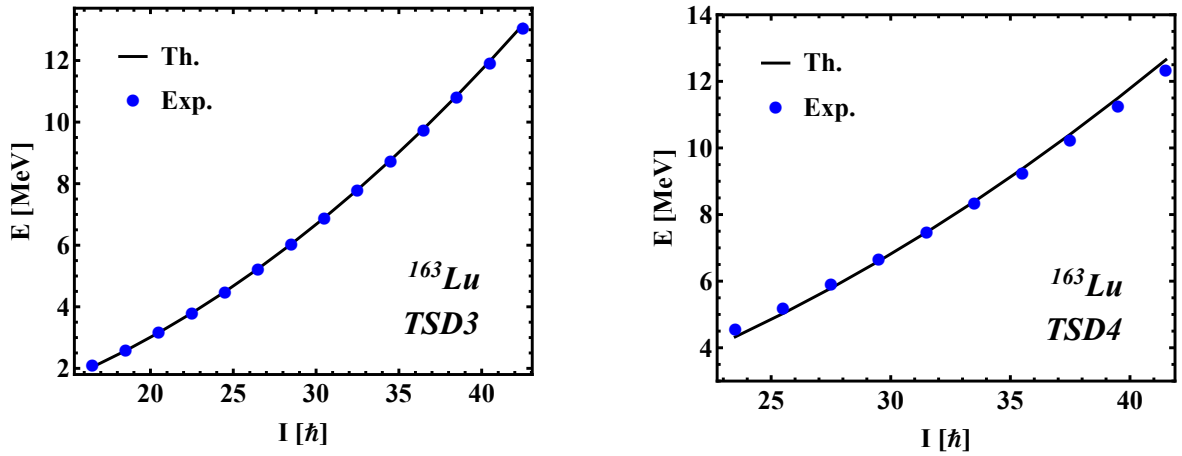

Figure 6: Comparison between theoretical and experimental excitation energies for third and fourth wobbling bands in ^{163}Lu within the W2 model. The theoretical results are obtained with the parameters listed in Table 3. Experimental data is taken from [88].

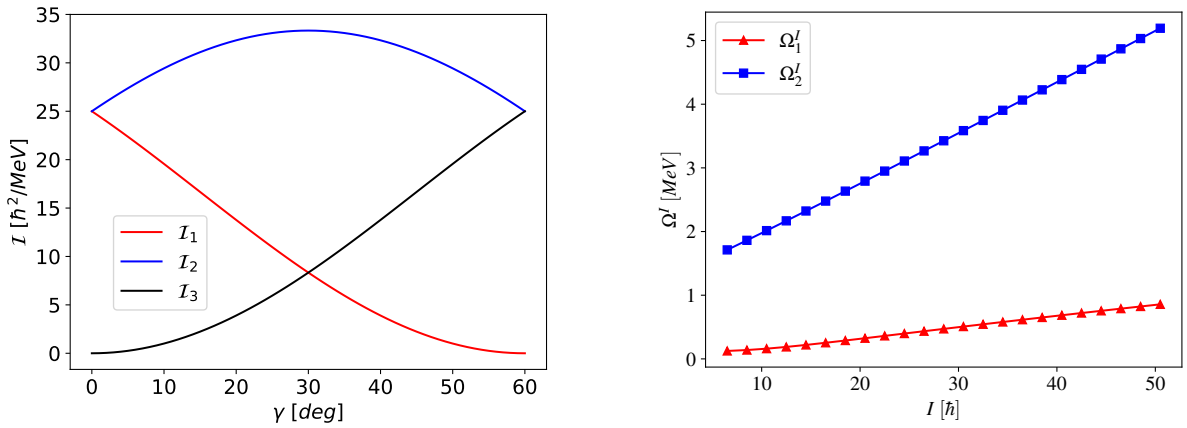

Figure 7: Left-side: The hydrodynamic moments of inertia [37] as function of the triaxiality parameter γ, for the positive interval $\gamma \in [0°, 60°]$, evaluated for a scale factor $\mathcal{I}_0 = 25$ MeV^{-1}. Right-side: The wobbling frequencies defined in Eq. 23 as function of total angular momentum, evaluated with the parameter set $\mathcal{P}$ which was obtained through the fitting procedure.

degeneracy by using an additional linear in the expression H. Since in Eq. 7 such a linear term is missing, an *ad-hoc* correction of the mean-field with the amount 0.6 MeV for the states in TSD_4 is necessary. As a result, the added shift simulates the breaking of parity symmetry. In contrast to this approach, using a microscopic formalism one starts with a single-particle basis generated by a mean-field without space reflection symmetry, followed by the calculation of the many-body wave-functions (being admixtures of both positive and negative parities). Restoration of the parity symmetry is achieved by selecting from all the wave-functions only the components with a definite parity (projecting the good parity), leading to a doublet structure of positive and negative parity states in the spectrum of H. Consequently, the bands TSD_2 and TSD_4 behave as a pair of parity partners, as defined in [89–91].

5.1 Interpretation of the parameter set $\mathcal{P}$

Performing the fitting procedure for the excitation energies of ^{163}Lu will result in the moments of inertia $\mathcal{I}_k$ that are given in Table 3, together with the single-particle potential strength V, and triaxiality parameter γ. Interpretation of their numerical values is mandatory in order to check whether the current formalism is valid or not.

Regarding the moments of inertia, it is clear that the axis of rotation for the energy ellipsoid is the 1-axis, as the largest MOI is $\mathcal{I}_1$, causing a maximal density distribution across this axis [35]. The MOI ordering is $\mathcal{I}_1 > \mathcal{I}_2 > \mathcal{I}_3$, and compared with the results of the previous work `W1`, the current 1-axis MOI is bigger than both $\mathcal{I}_1^{\mathrm{TSD1,2,3}} = 63.2\ \hbar^2/\mathrm{MeV}$ and $\mathcal{I}_1^{\mathrm{TSD4}} = 67\ \hbar^2/\mathrm{MeV}$ (data taken from Table 1 in Ref. [15]). This is expected, since here, the TSD_4 band is obtained by the coupling of a higher aligned j particle, driving the system to an even larger deformation. One must remember that these are the *effective* MOIs of the entire system, that is the triaxial-rotor + odd-particle. No spin dependence has been inferred for the MOIs, so a possible change in the MOIs ordering with the increase in spin I cannot be studied within the current description. Furthermore, this formalism does not contain microscopic terms, so no presumptions on what causes the obtained MOI ordering can be stated. Although, by working with a quadrupole deformed mean-field, the moments of inertia of the triaxial core should be indeed consistent with the hydrodynamic model. For the sake of completeness, Figure 7 shows the evolution of a hydro-dynamical set of MOIs with respect to the triaxiality parameter γ.

Concerning the triaxiality parameterγ, it has a positive value $\gamma = 22°$. This is consistent with the microscopic descriptions based on cranking mechanism for the potential energy surface (PES) of ^{163}Lu (discussion on PES was done in the previous sections). In fact, the agreement is quite good with the predicted deformed minima of $(\beta_2, \gamma) \approx (0.38, 20°)$ [19,68]. Comparing the current `W2` model with already existing descriptions which take γ to be fixed a-priori throughout the calculations (e.g., [37,69]), here γ is obtained through the fitting process in a self-consistent manner. Moreover, its value is slightly larger than the one obtained in `W1` formalism ($\gamma = 17°$). This might be due to the larger ratios $\mathcal{I}_1/\mathcal{I}_{2,3}$, which in the present case they appear to be bigger ($\mathcal{I}_1/\mathcal{I}_2 \approx 4.8$ for `W2`, compared to ≈ 3.2 in the previous approach W1).

Finally, the single-particle potential strength, which causes the odd-proton to move in the quadrupole deformed mean-field, has a value of $V = 2.1$ MeV. In `W1`, this parameter was $V^{\mathrm{TSD1,2,3}} = 3.1$ MeV and $V^{\mathrm{TSD4}} = 0.7$ MeV. An explanation for its decrease in the present case might be due to the upward shift in the energy caused by the un-favored partner, or due to the energetic shift of the parity partner, indicating a quenching effect on the quadrupole deformation of the triaxial system. Nevertheless, the obtained value seems

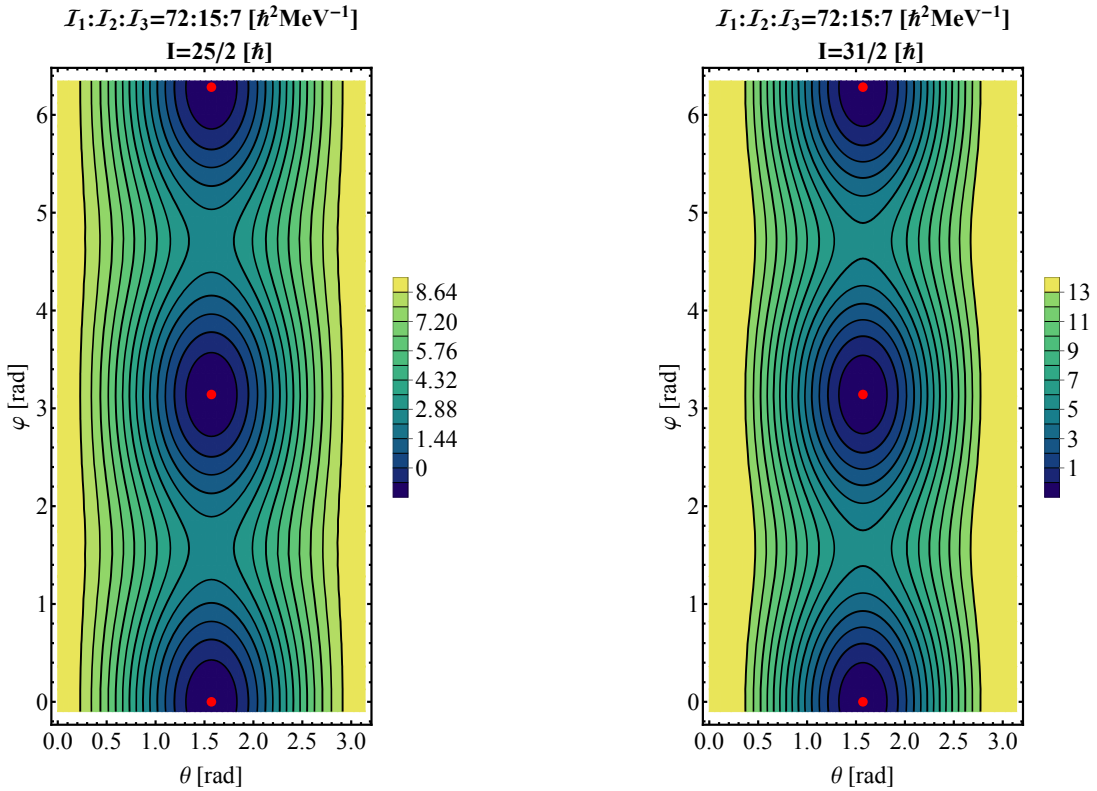

Figure 8: Contour plots with the energy function $\mathcal{H}$ given by Eq. 35 for a state in TSD_1 (left) and a state from TSD_2 (right). Calculations were performed with the numerical parameters obtained from the fitting procedure of the excitation energies. The minimum points for $\mathcal{H}$ are marked by red dots, and they represent the regions in space where the nucleus has a stable wobbling character. The darker *islands* also indicate a stable motion of the triaxial nucleus.

to be consistent with the previous calculations, the current value of V being close to the average value of V's from `W1`. Other interpretations [69] that were developed using a similar single-particle potential term in the Hamiltonian adopted values of around $V = 1.6$ MeV, however, that was for an isotope with smaller quadrupole deformation $\beta_2 = 0.18$. Interesting research using a single-j shell model which was aimed at obtaining a realistic expression for the deformation parameter has been performed in [92]. Therein, results for the potential strength of odd-A nuclei with similar mass, but different quasiparticle configurations were numerically obtained. Adoption of an equivalent description for the odd-j particle within `W2` could be done, and then compare results for a corresponding configuration. This could be the motivating factor for future work. Concluding this subsection, the obtained values of $\mathcal{P}$ seem to not only describe the wobbling spectrum of ^{163}Lu very well (see results in Figures 5 and 6), but they are also consistent with the previous formalism `W1`, or even with other interpretations from the literature.

5.2 Stability of the wobbling region

The expression for the classical energy function, which plays a crucial role in analyzing the nucleus's stability for a given rotational state, was presented in the previous section, through Eq. 35. This will be used within the present numerical calculations to pinpoint the regions in space where the minimal points of $\mathcal{H}$ exist. A special interest is devoted to the low-lying states from each of the four bands. Namely, for each band, a spin-state close to the band-head is chosen, then using the parameter set $\mathcal{P}$, a graphical representation in the (θ, φ)-coordinate space is realized, and in each case, the extremal points with minimum character are identified. These graphical representations are shown in Figures 8 and 9.

The four contour plots shown in Figures 8 and 9 have many similarities, suggesting common collective properties, but also differences which are caused by the fact that the minima have different depths. A common feature consists in that the equi-energy curves surround a sole minimum for low values in energy, but as the energy increases, the trajectories go around all minima, the lack of localization indicating unstable wobbling motion. The unstable regions might also relate to phase transitions, where the nucleus can undergo a major change in its rotational character. This aspect will also be discussed in the next subsection, devoted to the 3-dimensional representation of the energy ellipsoid and the classical trajectories of the triaxial system.

Regarding the minimum points (marked by red dots on the contour plots), their position remains unchanged

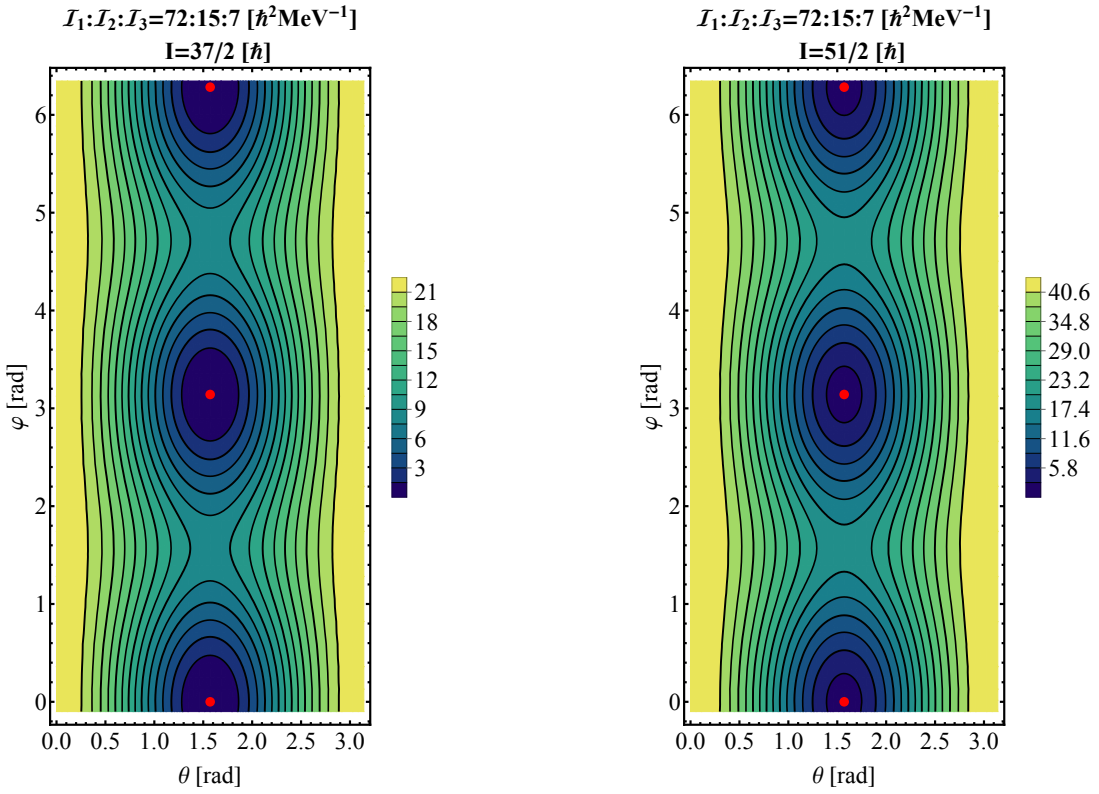

Figure 9: Contour plots with the energy function $\mathcal{H}$ given by Eq. 35 for a state in TSD_3 (left) and a state from TSD_4 (right). Calculations were performed with the numerical parameters obtained from the fitting procedure of the excitation energies. The minimum points for $\mathcal{H}$ are marked by red dots, and they represent the regions in space where the nucleus has a stable wobbling character. The darker *islands* also indicate a stable motion of the triaxial nucleus.

for all four bands and any rotational state I, as long as the MOI order stays the same. Remarkable is the fact that only with the obtained set of parameters (the current MOI ordering) it was possible to define contours with stable motion (marked by the darker regions). Indeed, if the two ratios $\mathcal{I}_1/\mathcal{I}_2$ and $\mathcal{I}_2/\mathcal{I}_3$ would have been smaller, a larger unstable region would prevail (with islands of maximal character), constraining thus the stable wobbling motion. This could indicate the fact that the single-particle term $T_{\text{s.p.}}$ from $\mathcal{H}$ is sensitive to larger triaxiality, and only for certain values will the system achieve a stable motion characterized by large deformation (see Eq. 36).

An additional step consists in the analysis of the energy function, more precisely to see its evolution in one of the minimum points with respect to the angular momentum I. As it was already observed from the contour plots shown in Figures 8-9, the depth of the minima differs from one spin state to another, so it would be useful to have a quantitative view on that change. By fixing $\mathcal{H}$ in one of its critical points (e.g., the minimum $p_{\min}(\theta,\varphi) = (\frac{\pi}{2}, 0)$), the angular momentum I was varied within a large interval, and the evolution of $\mathcal{H}$ was evaluated. Graphical representation is shown in Figure 10.

As it can be seen from Figure 10, the classical energy $\mathcal{H}$ is an increasing function of angular momentum, which is to be expected, since the wobbling energies of the four bands increase with respect to the increase in spin. The negative values of $\mathcal{H}$ for low-lying wobbling states do not indicate that the nucleus has negative energy states since *the rest* of the nucleus' energy is also given by the single-particle energy ϵ_j terms and the phononic $\mathcal{F}^I_{n_{w_1} n_{w_2}}$ terms.

Another useful insight would be the study of the classical energy function $\mathcal{H}$ for the obtained parameter set, as a function of the polar angles (θ, φ). This can be achieved by choosing a minimum point, keeping one of the polar coordinates fixed, and then let the other one vary across its corresponding interval. For ^{163}Lu, such a graphical representation was done for the point $p_{\min} = \left(\frac{\pi}{2}, 0\right)$ (that is the bottom-most red dot from each of the four contour plots depicted in Figures 8-9). Results can be seen in Figure 11.

5.3 Comment on the wobbling nature of ^{163}Lu

It is worthwhile discussing the results obtained regarding the wobbling spectrum of ^{163}Lu. Indeed, by using a fitting procedure that minimized the χ^2 function, it was possible to find a parameter set $\mathcal{P}$ that provides an agreement with the observed experimental data. However, in the current state, there is no clear evidence on

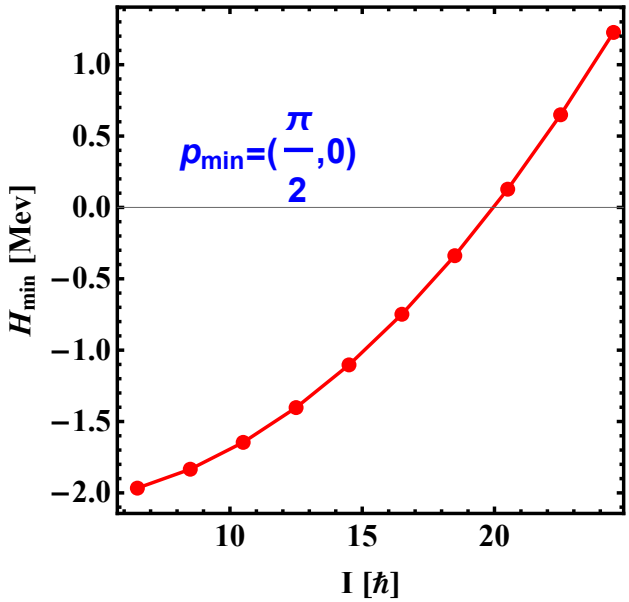

Figure 10: The change in the minimum depth of $\mathcal{H}$, evaluated in the point $(\theta, \varphi) = (\frac{\pi}{2}, 0)$, for the obtained parameter set $\mathcal{P}$.

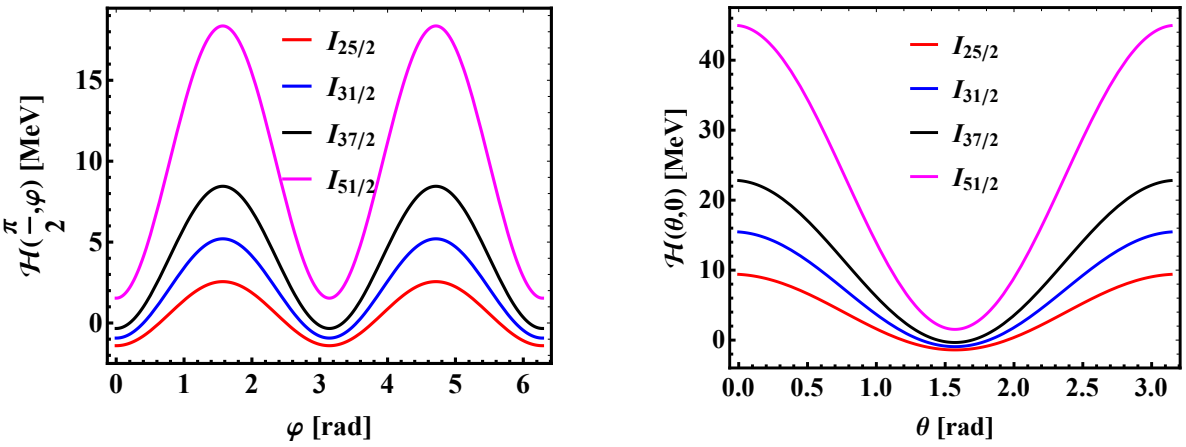

Figure 11: The energy function $\mathcal{H}$, evaluated in one of its minimum points, as a function of the polar coordinates. One coordinate is fixed while the other one is varied within its interval of existence. For $\theta \in [0, \pi]$ and $\varphi \in [0, 2\pi]$. The chosen minimum is $p_{\min} = \left(\frac{\pi}{2}, 0\right)$. Each spin state corresponds to one of the four triaxial bands of ^{163}Lu.

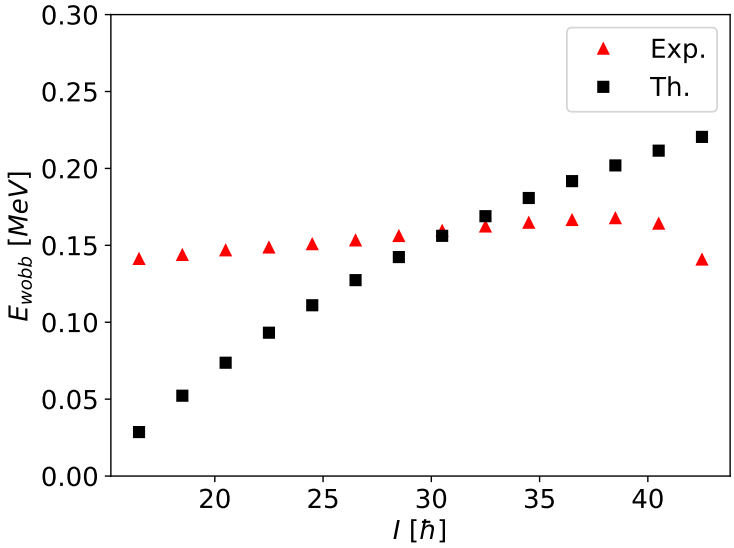

Figure 12: The wobbling energies for ^{163}Lu given as $E_{\text{wob}} = E_1(I) - \frac{1}{2}(E_0(I+1) + E_0(I-1))$. According to the current `W2` formalism, the sets of energies E_1 belong to TSD_3, while E_0 correspond to TSD_2. Experimental data is taken from [88]. Theoretical values were calculated with the parameter set $\mathcal{P}$.

whether the formalism `W2` predicts a TW or an LW behavior for the nucleus. According to [35], the wobbling character is given by the coupling of the odd particle which aligns parallel (LW) or perpendicular (TW) to the axis with the largest MOI. But to see this within the measured data, the interpretation of the wobbling energy as it was defined in Eq. 3 must be performed. As such, according to the definition, one has to subtract an energy state within the first excited wobbling band (the one-wobbling-phonon band) from the average of its adjacent energies that belong to the yrast partner. In the present calculations, the first excited state is TSD_3, with its yrast partner being the band TSD_2. Following this procedure, both the experimental wobbling energies, as well as the theoretical ones were calculated according to the Eq. 3. The obtained results are plotted in Figure 12.

From the behavior of E_{wob} from Figure 12, it can be seen that the theoretical wobbling spectrum is an increasing function of angular momentum I, suggesting that ^{163}Lu would have an LW character. This contrasts the current interpretation on which the wobbling energies are decreasing functions with respect to increasing angular momentum. However, within those formalisms [35, 70], the wobbling energies are obtained from TSD_2 and TSD_1, since the one-wobbling-phonon band is TSD_2, in contradistinction to the present `W2` model, where the first excited wobbling band is TSD_3.

Analyzing the experimental data points from Figure 12, a slight increase with spin can also be observed, suggesting as well that the coupling scheme in ^{163}Lu achieves an LW character. Indeed, from the lower limit of around $11/2\ \hbar$ and up to a spin of about $39/2\ \hbar$, the energy is increasing, then it starts to decrease once $I \geq 39/2\ \hbar$. The increasing behavior of the theoretical data also appears to be quenched in the high-spin limit, indicating that indeed, once the nucleus reaches high rotational states, a change in the wobbling regime might emerge, and the nucleus can transition from a wobbling regime (LW) to another (TW).

Referring back to the the case of ^{183}Au [27], the two observed wobbling bands are based on different alignments: the $\pi(i_{13/2})$ nucleon (for the so-called *positive parity band*) and the $\pi(h_{9/2})$ nucleon (for the *negative-parity* band) coupled to a triaxial rotor, respectively. The remarking aspect of this research is that within a PRM model amended with the HFA (harmonic frozen alignment) approximation, it is implied that the configurations of both bands have a transverse (TW) character. However, the wobbling energies E_{wob} in these bands have different behavior with respect to the increase of angular momentum. Namely, E_{wob} increases (decreases) with spin for the positive (negative) parity configurations (see Figures 3 and 5 from [27]). This indicates that an increasing/decreasing behavior for E_{wob} is not enough evidence for asserting a wobbling character on a triaxial nucleus (at least, not without some strong constraints on the coupling scheme between the core and the odd particle).

Concluding this comment on the wobbling nature for ^{163}Lu, if the behavior of the wobbling energies with spin is the sole player in determining the wobbling character of a nucleus, then one could argue that indeed, based on the current results, ^{163}Lu behaves as a longitudinal wobbler. On the other hand, considering the newly obtained results discussed in the previous paragraphs, the evidence is not enough for making a clear assumption on which type of wobbling motion occurs.

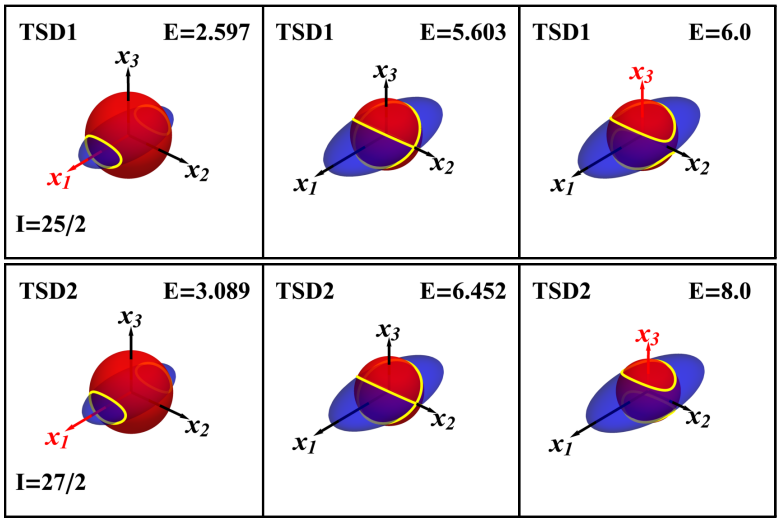

Figure 13: The nuclear trajectories of the system, evaluated for two spin states belonging to TSD_1 and TSD_2. Intersection lines marked by yellow color represents the actual orbits. Axis colored in red represents the direction along which the system rotates (it precesses). The left-most inset corresponds to the real excitation energy for that particular spin state I.

5.4 Classical trajectories - 3-dimensional representation

The final step of the present work is to obtain an insight into the classical features of the ^{163} triaxial nucleus in terms of its motion within the angular momentum space. As already mentioned, the trajectories are given by the intersection curves of the energy ellipsoid E given in Eq. 37 with the angular momentum sphere I^2 given in Eq. 38. In the 3-dimensional space generated by the three components of the angular momentum vector $\vec{I}$, these intersection curves characterize the motion of the system, as each curve will be oriented along with one of the three axes x_k , $k = 1, 2, 3$, suggesting a rotational motion (the precession of the total a.m.) around a particular direction preferred by the system.

The dependence of the classical trajectories on the angular momenta as well as on energies is thus analyzed in `W2`. Indeed, when the model Hamiltonian is diagonalized for a given I, a set of $2I + 1$ energies are obtained. Therefore, it is justified to study the evolution of trajectories when the energy of the nucleus is increasing. The curves are represented as the manifold given by the intersection of the two constants of motion, that is E and I^2. An example of such trajectories are depicted in Figures 13-14.

Each row from the Figures 13-14 represents a rotational state within a band. A low-lying spin state was chosen from each band in particular as an example. The left inset within each row represents the real excitation energy for the state I at which the energy ellipsoid is evaluated. It can be seen that two distinct (but symmetric) trajectories are observed along the 1-axis, for all four states. This suggests that the states of the triaxial nucleus are obtained from the rotation of the angular momentum along x_1. Indeed, for low energies, the rotation is more pronounced along the x_1- and $-x_1$-axes. As the energy of the nucleus increases, the two trajectories approach each other, which results in a tilted rotation axis corresponding to both curves. The tilted axis implies that the rotation axis is being misaligned, the rotational axis moving away from its *equilibrium point*, marking the tilted-axis-rotation. Note that this picture is fully consistent with the one described by Lawrie et al. [93]. Further increase in energy will result in the two trajectories intersect with each other. That particular point where the intersection between the two orbits occurs is marked in the middle inset from each figure. Consequently, the intersection of these two orbits marks an unstable motion within the system. Finally, when the energy increases even more, beyond this *critical point*, one arrives again in a two-trajectories regime but with a different rotation axis, lying closer to the x_3 axis. This case is shown in the right inset within each figure, where the axis x_3 is marked by red color, signaling the change in the rotational mode of the nucleus. However, it is worth noting that such energies are way too large for such a phase transition to occur naturally in ^{163}Lu. For example, in the case of $I_{25/2} \in TSD_1$, the energy at which ^{163}Lu undergoes a phase transition with regards to the rotational mode is close to 5.6 MeV (middle inset for TSD_1 from Figure 8), but the real excitation energy which corresponds to this state is half that (left inset for TSD_1 from Figure 13). Nevertheless, it is a remarkable fact that with the current model, a phase transition between rotational modes in a triaxial nucleus can be identified. A proper microscopic formalism based on this current approach might also provide a more detailed picture with regards to the allowed trajectories for the system.

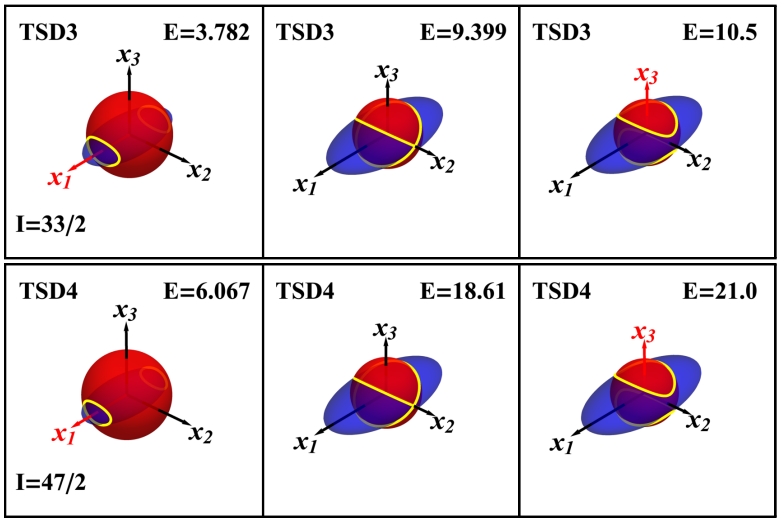

Figure 14: The nuclear trajectories of the system, evaluated for two spin states belonging to TSD_3 and TSD_4. Intersection lines marked by yellow color represents the actual orbits. Axis colored in red represents the direction along which the system rotates (it precesses). The left-most inset corresponds to the real excitation energy for that particular spin state I.

6 Conclusions & Outlook

The purpose of the present work was two-fold. On one hand, a detailed overview regarding the current experimental observations for wobbling motion in both even- and odd-mass nuclei across several mass regions was made in the introductory part (covered in Section 2.1). This was accompanied by a brief mention of the theoretical methods that are used for the microscopic/macroscopic description of the wobbling phenomenon (see Section 2.2). Also in the first part of the paper, a schematic analysis on the characteristics of the wobbling motion was made, which concerned the particle-core configurations in a longitudinal/transverse wobbler. Therein, it was shown that depending on the alignment of the odd quasiparticle with the triaxial core, a certain wobbling regime will prevail, thus concluding the introduction.

On the other hand, the second objective of the current paper was to extend a previous model that describes the ^{163}Lu using a re-interpretation of its four wobbling bands $TSD_{1,2,3,4}$. The previous model (denoted here by `W1`) introduced the concept of signature partners between the bands TSD_1 and TSD_2. One showed that the nucleus can be described as a particle that is moving in a quadrupole deformed mean field generated by the core. In `W1`, there was an $i_{13/2}$ proton involved in the particle-rotor-coupling for the description of the first three triaxial bands, and another proton with negative parity, i.e., the $\pi(h_{9/2})$ intruder for band TSD_4. Based on `W1`, a new approach was developed here as an extension, denoted throughout the paper by `W2`. The new formalism starts with the same Hamiltonian, however, in the present case a single trial function is constructed to admit eigenstates with both positive and negative parity. Indeed, despite the fact that TSD_4 is of an opposite parity than the first three, all bands are described by the coupling of a unique single-particle ($i_{13/2}$ with positive parity $\pi_j = +1$) to the core states of positive parity for $TSD_{1,2,3}$ and core states of negative parity for TSD_4. The coupling schemes for the wobbling bands within `W2` were denoted throughout the paper by C_1', C_2', C_3'. From the quantal Hamiltonian specific to a Particle Rotor Model (given by Eq. 7), by applying a Time-Dependent Variational Principle (TDVE) as in Eq. 12 with the trial function carefully chosen so that it allows a mixture of both positive and negative parity states, a set of analytical expressions for the excitation energies of each band were obtained (defined in Eq. 25). The excitation energies comprise a term that represents the classical energy function, obtained as the average of the Hamiltonian with the trial wave function (Eq. 27). A second term has a phonon character (Eq. 26), being composed of two wobbling frequencies that were obtained from the solutions to a dispersion-like equation as defined in Eq. 18.

From the theoretical formalism of the excitation energies of ^{163}Lu, a set of free parameters emerged, containing the three moments of inertia, the single-particle potential strength V, and the triaxiality parameter γ. They were obtained through a fitting procedure which was done for all four bands, unlike the previous `W1` approach. The resulted parameter set provides an impressive agreement between the existing theoretical and experimental data concerning the wobbling spectrum of this isotope, with an r.m.s. of about 79 keV. An interpretation of the numerical values for the obtained parameters was done in Section 5.1, and indeed, the obtained values are consistent with other formalisms from the literature. Furthermore, the study of the classical energy function was done in a polar coordinate system, obtaining the contour plots for spin states belonging to each triaxial band (Section 5.2). The critical points from those contour maps indicate stability in terms of wobbling behavior

(with closed orbits signaling stable trajectories). Unstable regions also emerge at high rotational energies. An additional comment on the wobbling nature of ^{163}Lu was made (see Section 5.3), and an analysis of the wobbling energy behavior with spin showed that the increasing trend might indicate a longitudinal character. Lastly, by intersecting the angular momentum sphere with the energy ellipsoid, the classical trajectories can be obtained. The results of this 3-dimensional representation are discussed throughout Section 5.4. From the graphical illustrations, three situations might occur for any given spin state of ^{163}Lu. i) At low energies, the rotation axis is either the 1-axis or the -1-axis, resulting in two trajectories along this axis. ii) At a particular energy - *critical energy* - the two orbits get close to each other until they intersect, marking the point of unstable motion for the nucleus. iii) If the energy increases even more, then the triaxial nucleus performs a tilted-axis-rotation, where the rotational axis slowly moves away from x_1, approaching x_3 and thus becoming misaligned. The change from one step to the other marks a phase transition. When the nucleus undergoes a transformation with regards to its rotational behavior it is actually changing its wobbling regime. Remarkable the fact that the current semi-classical approach is able to predict the change in the wobbling regime, this being of large interest in the nuclear community since evidence of such behavior was missing.

Concluding the present work, this newly developed formalism proves to be a successful tool for accurately describing the wobbling spectrum of ^{163}Lu and also for providing an insight into the rotational motion of the nuclear system with respect to its total spin.

Acknowledgments

This work was supported by UEFISCU, through the project **PCE-16/2021**.

A Appendix - Workflow Diagrams

The two models described in Section 2, namely the formalism `W1` (see Section 3.1) and `W2` (see Section 3.2) are schematically represented, based on the discussions made for each of the two approaches. The `W1` mode corresponds to the work given in Refs. [15,64], and the `W2` corresponds to the formalism developed in the present paper. For the formalism `W1`, the diagram is shown in Figure 15, while for the newly developed approach `W2`, the diagram is shown in Figure 16.

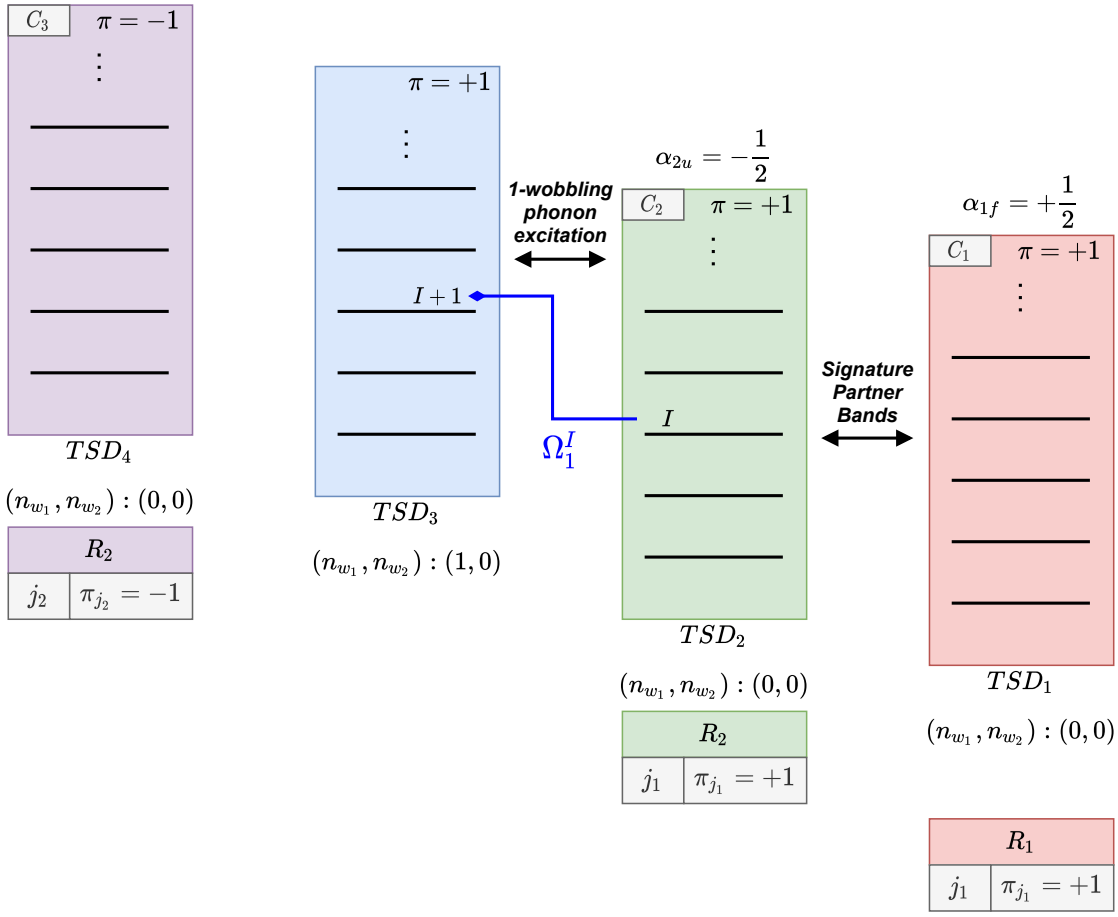

Figure 15: Schematic representation of the band structure adopted for ^{163}Lu in the `W1` model. For each band, the wobbling phonon numbers are shown. The main features and linking properties between bands are represented with arrows. The bottom part shows the coupling scheme (the core and the valence nucleon) for each wobbling band as described in the text, namely C_1, C_2, C_3 (see Section 3.1). The blue arrow marks the activation of TSD_3 states via the phonon operator.

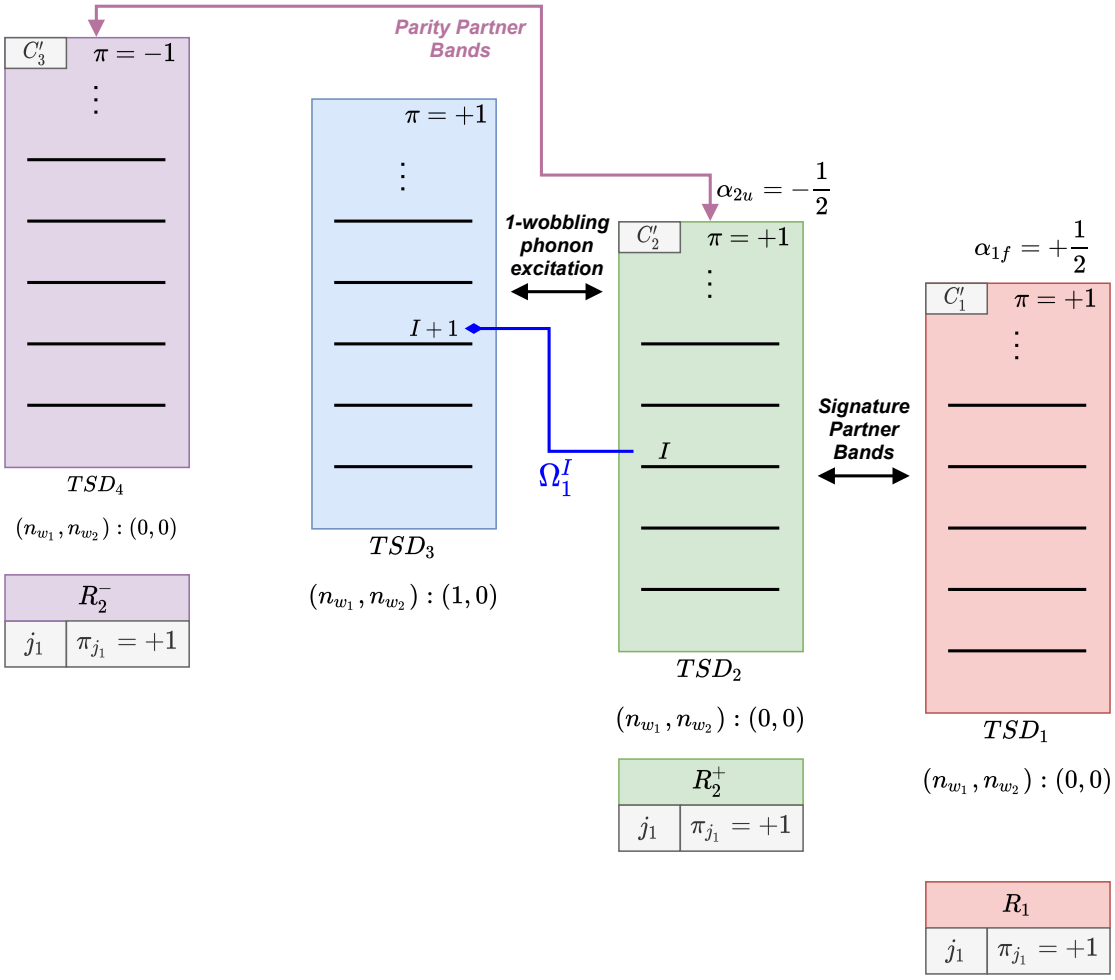

Figure 16: Schematic representation of the band structure adopted for ^{163}Lu in the `W2` model. For each band, the wobbling phonon numbers are shown. The main features and linking properties between bands are represented with arrows. The bottom part shows the coupling scheme (the core and the valence nucleon) for each wobbling band as described in the text, namely C'_1, C'_2, C'_3. The blue arrow marks the activation of TSD_3 states via the phonon operator.

References

[1] Peter Möller, Ragnar Bengtsson, B Gillis Carlsson, Peter Olivius, and Takatoshi Ichikawa. *Physical review letters*, 97(16):162502, 2006.

[2] Peter Möller, Arnold J Sierk, Takatoshi Ichikawa, Akira Iwamoto, Ragnar Bengtsson, Henrik Uhrenholt, and Sven Åberg. *Physical Review C*, 79(6):064304, 2009.

[3] I Hamamoto and H Sagawa. *Physics Letters B*, 201(4):415–419, 1988.

[4] R Bengtsson, H Frisk, FR May, and JA Pinston. *Nuclear Physics A*, 415(2):189–214, 1984.

[5] J Stachel, N Kaffrell, E Grosse, H Emling, H Folger, R Kulessa, and D Schwalm. *Nuclear Physics A*, 383(3):429–467, 1982.

[6] Stefan Frauendorf and Jie Meng. *Nuclear Physics A*, 617(2):131–147, 1997.

[7] Aage Niels Bohr and Ben R Mottelson. *Nuclear Structure (In 2 Volumes)*.

[8] BW Xiong and YY Wang. *Atomic Data and Nuclear Data Tables*, 125:193–225, 2019.

[9] VI Dimitrov, S Frauendorf, and F Dönau. *Physical review letters*, 84(25):5732, 2000.

[10] T Koike, K Starosta, CJ Chiara, DB Fossan, and DR LaFosse. *Physical Review C*, 67(4):044319, 2003.

[11] J Meng, J Peng, SQ Zhang, and S-G Zhou. *Physical Review C*, 73(3):037303, 2006.

[12] AA Raduta, Al H Raduta, and CM Petrache. *Journal of Physics G: Nuclear and Particle Physics*, 43(9):095107, 2016.

[13] CM Petrache, BF Lv, A Astier, E Dupont, YK Wang, SQ Zhang, PW Zhao, ZX Ren, J Meng, PT Greenlees, et al. *Physical Review C*, 97(4):041304, 2018.

[14] BF Lv, CM Petrache, QB Chen, J Meng, A Astier, E Dupont, P Greenlees, H Badran, T Calverley, DM Cox, et al. *Physical Review C*, 100(2):024314, 2019.

[15] AA Raduta, R Poenaru, and CM Raduta. *Journal of Physics G: Nuclear and Particle Physics*, 47(2):025101, 2020.

[16] Gudrun B Hagemann and Ikuko Hamamoto. *Nuclear Physics News*, 13(3):20–24, 2003.

[17] SW Ødegård, GB Hagemann, DR Jensen, M Bergström, B Herskind, G Sletten, S Törmänen, JN Wilson, PO Tjøm, I Hamamoto, et al. *Physical review letters*, 86(26):5866, 2001.

[18] DR Jensen, GB Hagemann, I Hamamoto, SW Ødegård, B Herskind, G Sletten, JN Wilson, K Spohr, H Hübel, P Bringel, et al. *Physical review letters*, 89(14):142503, 2002.

[19] D Ringkøbing Jensen, GB Hagemann, I Hamamoto, SW Ødegård, M Bergström, B Herskind, G Sletten, S Törmänen, JN Wilson, PO Tjøm, et al. *Nuclear Physics A*, 703(1-2):3–44, 2002.

[20] H Schnack-Petersen, Ragnar Bengtsson, RA Bark, P Bosetti, A Brockstedt, H Carlsson, LP Ekström, GB Hagemann, B Herskind, F Ingebretsen, et al. *Nuclear Physics A*, 594(2):175–202, 1995.

[21] S Biswas, R Palit, S Frauendorf, U Garg, W Li, GH Bhat, JA Sheikh, J Sethi, S Saha, Purnima Singh, et al. *The European Physical Journal A*, 55(9):1–7, 2019.

[22] James Till Matta. Transverse wobbling in 135 pr. In *Exotic Nuclear Excitations: The Transverse Wobbling Mode in 135 Pr*, pages 77–93. Springer, 2017.

[23] N Sensharma, U Garg, S Zhu, AD Ayangeakaa, S Frauendorf, W Li, GH Bhat, JA Sheikh, MP Carpenter, QB Chen, et al. *Physics Letters B*, 792:170–174, 2019.

[24] S Chakraborty, HP Sharma, SS Tiwary, C Majumder, AK Gupta, P Banerjee, S Ganguly, S Rai, S Kumar, A Kumar, et al. *Physics Letters B*, 811:135854, 2020.

[25] C M Petrache. *LNL Annual Report*, 2018.

[26] J Timár, QB Chen, B Kruzsicz, D Sohler, I Kuti, SQ Zhang, J Meng, P Joshi, R Wadsworth, K Starosta, et al. *Physical review letters*, 122(6):062501, 2019.

[27] S Nandi, G Mukherjee, QB Chen, S Frauendorf, R Banik, Soumik Bhattacharya, Shabir Dar, S Bhattacharyya, C Bhattacharya, S Chatterjee, et al. *Physical Review Letters*, 125(13):132501, 2020.

[28] N Sensharma, U Garg, QB Chen, S Frauendorf, DP Burdette, JL Cozzi, KB Howard, S Zhu, MP Carpenter, P Copp, et al. *Physical review letters*, 124(5):052501, 2020.

[29] S Guo, XH Zhou, CM Petrache, EA Lawrie, S Mthembu, YD Fang, HY Wu, HL Wang, HY Meng, GS Li, et al. *arXiv preprint arXiv:2011.14354*, 2020.

[30] JH Hamilton, SJ Zhu, YX Luo, AV Ramayya, S Frauendorf, JO Rasmussen, JK Hwang, SH Liu, GM Ter-Akopian, AV Daniel, et al. *Nuclear Physics A*, 834(1-4):28c–31c, 2010.

[31] YX Luo, JH Hamilton, AV Ramaya, JK Hwang, SH Liu, JO Rasmussen, S Frauendorf, GM Ter-Akopian, AV Daniel, Yu Ts Oganessian, et al. Triaxial and triaxial softness in neutron rich ru and pd nuclei. In *Exotic Nuclei: EXON-2012*, pages 215–224. World Scientific, 2013.

[32] CM Petrache, PM Walker, S Guo, QB Chen, S Frauendorf, YX Liu, RA Wyss, D Mengoni, YH Qiang, A Astier, et al. *Physics Letters B*, 795:241–247, 2019.

[33] YK Wang, FQ Chen, and PW Zhao. *Physics Letters B*, 802:135246, 2020.

[34] QB Chen, S Frauendorf, and CM Petrache. *Physical Review C*, 100(6):061301, 2019.

[35] S Frauendorf and F Dönau. *Physical Review C*, 89(1):014322, 2014.

[36] Ikuko Hamamoto. *Physical Review C*, 65(4):044305, 2002.

[37] Kosai Tanabe and Kazuko Sugawara-Tanabe. *Physical Review C*, 73(3):034305, 2006.

[38] Shi Wen-Xian and Chen Qi-Bo. *Chinese Physics C*, 39(5):054105, 2015.

[39] AS Davydov and GF Filippov. *Nuclear Physics*, 8:237–249, 1958.

[40] Yoshifumi R Shimizu and Masayuki Matsuzaki. *Nuclear Physics A*, 588(3):559–596, 1995.

[41] Masayuki Matsuzaki, Yoshifumi R Shimizu, and Kenichi Matsuyanagi. *Physical Review C*, 65(4):041303, 2002.

[42] Masayuki Matsuzaki, Yoshifumi R Shimizu, and Kenichi Matsuyanagi. *The European Physical Journal A-Hadrons and Nuclei*, 20(1):189–190, 2003.

[43] Masayuki Matsuzaki and Shin-Ichi Ohtsubo. *Physical Review C*, 69(6):064317, 2004.

[44] Masayuki Matsuzaki, Yoshifumi R Shimizu, and Kenichi Matsuyanagi. *Physical Review C*, 69(3):034325, 2004.

[45] Yoshifumi R Shimizu, Masayuki Matsuzaki, and Kenichi Matsuyanagi. *Physical Review C*, 72(1):014306, 2005.

[46] Yoshifumi R Shimizu, Takuya Shoji, and Masayuki Matsuzaki. *Physical Review C*, 77(2):024319, 2008.

[47] Takuya Shoji and Yoshifumi R Shimizu. *Progress of theoretical physics*, 121(2):319–355, 2009.

[48] QB Chen, SQ Zhang, PW Zhao, and J Meng. *Physical Review C*, 90(4):044306, 2014.

[49] QB Chen, SQ Zhang, J Meng, et al. *Physical Review C*, 94(5):054308, 2016.

[50] S Mukhopadhyay, D Almehed, U Garg, S Frauendorf, T Li, PV Madhusudhana Rao, X Wang, SS Ghugre, MP Carpenter, S Gros, et al. *Physical review letters*, 99(17):172501, 2007.

[51] Bin Qi, SQ Zhang, J Meng, SY Wang, and S Frauendorf. *Physics Letters B*, 675(2):175–180, 2009.

[52] Makito Oi, Ahmad Ansari, Takatoshi Horibata, and Naoki Onishi. *Physics Letters B*, 480(1-2):53–60, 2000.

[53] AA Raduta, R Poenaru, and L Gr Ixaru. *Physical Review C*, 96(5):054320, 2017.

[54] AA Raduta, CM Raduta, and R Poenaru. *Journal of Physics G: Nuclear and Particle Physics*, 48(1):015106, 2020.

[55] K Tanabe and K Sugawara-Tanabe. *Physics Letters B*, 34(7):575–578, 1971.

[56] Kosai Tanabe and Kazuko Sugawara-Tanabe. *Physical Review C*, 77(6):064318, 2008.

[57] Mitsuhiro Shimada, Yudai Fujioka, Shingo Tagami, and Yoshifumi R Shimizu. *Physical Review C*, 97(2):024318, 2018.

[58] Kenji Hara and Yang Sun. *International Journal of Modern Physics E*, 4(04):637–785, 1995.

[59] PW Zhao, P Ring, and J Meng. *Physical Review C*, 94(4):041301, 2016.

[60] M Konieczka, Markus Kortelainen, and W Satuła. *Physical Review C*, 97(3):034310, 2018.

[61] AA Raduta, R Budaca, and CM Raduta. *Physical Review C*, 76(6):064309, 2007.

[62] AA Raduta, R Poenaru, and Al H Raduta. *Journal of Physics G: Nuclear and Particle Physics*, 45(10):105104, 2018.

[63] R Budaca. *Physical Review C*, 97(2):024302, 2018.

[64] AA Raduta, R Poenaru, and CM Raduta. *Physical Review C*, 101(1):014302, 2020.

[65] Tord Bengtsson. *Nuclear Physics A*, 512(1):124–148, 1990.

[66] A Görgen, RM Clark, M Cromaz, P Fallon, GB Hagemann, H Hübel, IY Lee, AO Macchiavelli, G Sletten, D Ward, et al. *Physical Review C*, 69(3):031301, 2004.

[67] GB Hagemann. *Acta Physica Polonica B*, 36(4):1043, 2005.

[68] DR Jensen, GB Hagemann, I Hamamoto, B Herskind, G Sletten, JN Wilson, SW Ødegård, K Spohr, H Hübel, P Bringel, et al. *The European Physical Journal A-Hadrons and Nuclei*, 19(2):173–185, 2004.

[69] Kosai Tanabe and Kazuko Sugawara-Tanabe. *Physical Review C*, 95(6):064315, 2017.

[70] S Frauendorf. *Physical Review C*, 97(6):069801, 2018.

[71] Kosai Tanabe and Kazuko Sugawara-Tanabe. *Physical Review C*, 97(6):069802, 2018.

[72] Yang Sun, Shuxian Wen, et al. *Physical Review C*, 50(5):2351, 1994.

[73] AM Khalaf, Hayam Yassin, and Eman R Abo Elyazeed. *Journal: Journal Of Advances In Physics*, 11(1), 2015.

[74] VS Uma and Alpana Goel. *The European Physical Journal Plus*, 130(6):1–6, 2015.

[75] HM Mittal and Anshul Dadwal. In *Proceedings of the DAE-BRNS Symp. on Nucl. Phys*, volume 61, page 134, 2016.

[76] Ikuko Hamamoto and Ben Mottelson. *Physics Letters B*, 127(5):281–285, 1983.

[77] Ikuko Hamamoto. *Physics Letters B*, 193(4):399–404, 1987.

[78] Ikuko Hamamoto. *Physica Scripta*, 91(2):023004, 2016.

[79] S Torilov, S Thummerer, W Von Oertzen, Tz Kokalova, G De Angelis, HG Bohlen, A Tumino, M Axiotis, E Farnea, N Marginean, et al. *The European Physical Journal A-Hadrons and Nuclei*, 19(3):307–317, 2004.

[80] ME Debray, MA Cardona, D Hojman, AJ Kreiner, M Davidson, J Davidson, H Somacal, G Levinton, DR Napoli, S Lenzi, et al. *Physical Review C*, 62(2):024304, 2000.

[81] AA Radutaa and CM Radutab. *arXiv preprint arXiv:0903.0076*, 2009.

[82] AA Raduta and CM Raduta. *Annals of the University of Craiova, Physics*, 21(1):28–53, 2011.

[83] J Meyer-ter Vehn. *Nuclear Physics A*, 249(1):111–140, 1975.

[84] SY Wang, SQ Zhang, B Qi, J Peng, JM Yao, J Meng, et al. *Physical Review C*, 77(3):034314, 2008.

[85] J Peng, J Meng, and SQ Zhang. *Physical Review C*, 68(4):044324, 2003.

[86] T Koike, K Starosta, and I Hamamoto. *Physical review letters*, 93(17):172502, 2004.

[87] SY Wang, SQ Zhang, B Qi, and J Meng. *Physical Review C*, 75(2):024309, 2007.

[88] CW Reich and Balraj Singh. *Nuclear Data Sheets*, 111(5):1211–1469, 2010.

[89] RR Chasman. *Physics Letters B*, 96(1-2):7–10, 1980.

[90] AA Raduta, CM Raduta, and Amand Faessler. *Physics Letters B*, 635(2-3):80–84, 2006.

[91] AA Raduta, Al H Raduta, and CM Raduta. *Physical Review C*, 74(4):044312, 2006.

[92] Wang Shou-Yu, Qi Bin, and Zhang Shuang-Quan. *Chinese Physics Letters*, 26(5):052102, 2009.

[93] EA Lawrie, O Shirinda, and CM Petrache. *Physical Review C*, 101(3):034306, 2020.